# Modelling of Mixing and Mass Transfer Phenomena in Gas Agitated Reactors

by

Rakesh Kumar

DEPARTMENT OF MATERIALS AND METALLURGICAL ENGINEERING
Indian Institute of Technology, Kanpur
July, 1997.

Modelling of Mixing and Mass Transfer Phenomena in Gas Agitated Reactors

A Thesis Submitted

in Partial Fulfilment of the Requirements

for the Degree of

Master of Technology

by

Rakesh Kumar

(Roll No: 9520611)

to the

DEPARTMENT OF MATERIALS AND METALLURGICAL ENGINEERING

INDIAN INSTITUTE OF TECHNOLOGY KANPUR

July, 1997

MME-1997-M-KUM-MOD

CERTIFICATE

It is certified that the work contained in the thesis entitled "Modelling of Mixing and Mass Transfer Phenomena in Gas Agitated Reactors", by **Rakesh Kumar (Roll No: 9520611)**, has been carried out under our supervision and that this work has not been submitted elsewhere for a degree.

Dr. Bramha Deo 22 (7/97

Professor

Dept. of Materials and Metallurgical Engg.
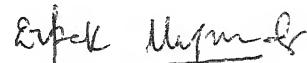
I.I.T.Kanpur

Dr. Dipak Mazumdar

Professor

Dept. of Materials and Metallurgical Engg.

I.I.T. Kanpur

July , 1997
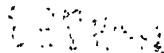
Dedicated

To

My Parents

ACKNOWLEDGEMENT

Contents

List of Figures

List of Tables

Nomenclature

a_P, a_N, a_E, a_W, a_S	:	coefficients of discretization equation
a_{nb}	:	neighbour point coefficients
g	:	acceleration due to gravity, (ms^{-2})
C_1, C_2, C_μ	:	constant of the $\kappa - \epsilon$ model
C_b	:	constant defined by eq. (2.22)
C_D	:	drag coefficient
d	:	diameter of rod/cylinder used in mass transfer correlations, (m)
D	:	diffusion coefficient, $(m^2 s^{-1})$
d_b	:	bubble diameter, (m)
F_z, F_r	:	interphase drag forces acting on the liquid in axial and radial directions respectively
κ	:	turbulence kinetic energy, $(m^2 s^2)$
K	:	mass transfer coefficient, (ms^1)
K_1	:	pre-exponent term of mass transfer correlation
K_2, K_3	:	exponent terms of mass transfer correlation
l	:	no. of bits in a string (chromosome length)
L	:	depth of liquid in vessel, (m)
n	:	number of data points for correlation prediction
N	:	number of bubbles in a particular trajectory in a given control volume
P	:	dynamic pressure with reference to the local hydrostatic pressure
P_c	:	cross over probability in GAs
P_m	:	mutation probability in GAs
P_s	:	population size in GAs
Pr	:	Prandtl number
Q_t	:	gas flow rate due to one trajectory, $(m^3 s^{-1})$
R	:	radius of the vessel, (m)
Re	:	Reynolds number

$Re_{Loc.}$: Reynolds number (local)

Re_t : Reynolds number (turbulent)

r : radial direction, (m)

Sc : Schmidt number

Sh : Sherwood number

t : time, (s)

$t_{r,m}$: residence time of the mth bubble

Tu : turbulence number

Δt : incremental time step, (s)

u : mean liquid velocity component in axial direction, (ms^{-1})

$\bar{u}$: r.m.s of the isotropic fluctuating velocity component, (ms^{-1})

U : instantaneous liquid velocity component in the axial direction, (ms^{-1})

U_b : resultant bubble velocity, (ms^{-1})

U_f : resultant instantaneous liquid velocity, (ms^{-1})

U_r : relative velocity vector, (ms^{-1})

v : horizontal component of mean liquid velocity, (ms^{-1})

V : horizontal component of instantaneous liquid velocity, (ms^{-1})

$V_{B,z}$: instantaneous bubble velocity in the axial direction, (ms^{-1})

$V_{B,r}$: instantaneous bubble velocity in the radial direction, (ms^{-1})

z : axial direction, (m)

ΔV_{cv} : volume of a control volume

α_g : gas volume fraction

α_l : liquid volume fraction

μ_l : liquid viscosity, $(kgm^{-1}s^{-1})$

ρ_g : gas density, (kgm^{-3})

ρ_l : liquid density, (kgm^{-3})

ϵ : rate of turbulence kinetic energy dissipation

Chapter 1

INTRODUCTION

1.1   Introduction to the Thesis

With an ever-rising demand for superior quality of steel at a competitive price, steel industries globally are on the look out for processes with the following features for a rapid attainment of end chemistry:

(i) Faster alloy dissolution to reduce processing time,

(ii) Higher alloy recoveries to have an edge on cost and cleanness front and

(iii) minimal thermal and particulate concentration gradient in the melt.

It can therefore be said that mass transfer and liquid mixing phenomena are perhaps the most critical operations in terms of quality steel production.

The melting and/or dissolution of solid additions in liquid steel melt is an integral unit operation in steel making industries. Large tonnage of ferro alloys and deoxidizer elements are added to liquid steel bath on a routine basis to adjust the chemistry of the melt and thus, produce a grade of steel to meet the customer requirements. Melting and dissolution of additions consume a large amount of energy and have an important bearing on the overall process economies. Quantitative frame works are therefore needed so that these can be predicted and also important informations on energy consumption, complete melting/dissolution times, optimal size ranges vis-a-vis the processing time etc. are known a-priori. This information, can help operators to run the melt shop more

economically and effectively.

In order to ensure a sound solidified product for customer, it is important that virtually no stratification of heat and mass takes place in the melt prior to casting. There has been a constant endeavour to exacerbate the rates of these transport process with obvious repercussions in the steel industries and thus, justifiably, these have been the subject of scientific research for more than two decades. Homogenization of melt with respect to composition and/or temperature is the fundamental requirement to guarantee a sound casting. Homogenization of steel prior to casting may be attained most economically by stirring liquid steel in a ladle (a cylindrical vessel with a slight taper towards bottom) in several ways. The most common configuration is bottom gas injection through a centre, or eccentric porous plug, or lance or tuyers. Liquid mixing in a gas-stirred bath occurs by the recirculatory and turbulent motion of the fluid induced by the injected gas. It is therefore important to develop a good understanding of the induced turbulent fluid motion in conjunction with the dispersion or homogenization process.

Mixing time is typically defined as the time within which, a vessel's liquid can reach a state of chemical and/or thermal stability. Mixing phenomena should investigated both theoretically and experimentally, but, owing to the large size of industrial processing units, high operating temperatures and visual opacity of liquid steel, it is practically impossible to carry out any meaningful experimental programme. Mathematical modelling provides a reasonable alternative to study the mixing phenomena in industrial processing units.

1.2 Previous work

1.2.1 Liquid mixing phenomena

So far as mathematical modelling of mixing times is concerned, different approached have been adopted by researchers. A summary of various procedures available for calculations has recently been presented by Mietz and Oeters [1]. From a conceptual stand point, two

different approaches have been applied and these include, modelling via numerical solu-
tions of the species conservation equation and the circulation time model. In conjunction
with mathematical modelling, experimental measurements of mixing time in water mod-
els and industrial argon stirred ladles were also carried out. Such measurements were
often applied to validate model predictions.

In presence of a two dimensional velocity field, the mass conservation of an inert tracer
i (e.g., m_i) can be expressed (in a cylindrical polar co-ordinate system) via the following
convection-turbulent diffusion equation:

$$\frac{\delta}{\delta t}(\rho m_i) + \frac{\delta}{\delta z}(\rho u m_i) + \frac{1}{r}\frac{\delta}{\delta r}(\rho u r m_i) = \frac{\delta}{\delta z}(\tau \frac{\delta m_i}{\delta z}) + \frac{1}{r}\frac{\delta}{\delta r}(\tau r \frac{\delta m_i}{\delta r}) \qquad (1.1)$$

The eddy diffusivity D_E ($=\frac{\tau}{\rho}$) and eddy kinematic viscosity, ν_E ($=\frac{\mu}{\rho}$), are conventionally
taken to be numerically equal. It is therefore apparent, that provided the flow parameters
(u and v) and turbulence quantities (μ_E) are known with reasonable certainty, mixing
time [viz., $m_i(z, r, t)$ fields] can be fairly accurately predicted because physically realistic
and accurate boundary conditions can be applied to Eq. (1.1). This has been a popular
approach in numerous mathematical modelling studies in which mixing phenomena have
been studied in aqueous as well as industrial gas stirred ladle system.
In a much earlier study, Szekely et al. [2] reported a combined theoretical and experi-
mental investigation of liquid mixing phenomena in industrial scale argon stirred ladles.
Mixing rates in three different size industrial ladles (viz., 7, 40, and 60 t) were measured
for various operating conditions by monitoring a transient local concentration of a ra-
dio active tracer addition. In conjunction with their experimental work, they predicted
mixing times through solution of Eq. (1.1) via a two dimensional elliptic, turbulent flow
model. Despite some simplifying assumptions, experimental measurements and numeri-
cal predictions were found to be in a reasonably good agreement. Similar observations on
water models of argon-stirred ladle have also been reported by Ying et al. [3], Salcudean
and co-workers [4], Mazumdar and Guthrie [5] and more recently by Joo and Guthrie
[6]. Computational studies of mixing phenomena in industrial size and water model la-
dles confirm that gas flow rate and vessel geometry affect mixing considerably and that

mixing rate vary significantly from one location to another in such gas stirred vessels.

In subsequent investigation El-Kaddah and Szekely [7] improved their earlier hydrodynamic model to predict the turbulent flow fields in 6 and 40t industrial ladles. Embodying the predicted flow parameters and turbulence quantities in the species conservation equation and invoking some thermodynamic equilibrium relationship, desulphurisation kinetics in the industrial argon stirred ladle were numerically predicted and reasonably good agreement with experimental measurements was demonstrated.

Mixing phenomena in gas stirred ladles designed for single and duel plug bubbling operations was reported recently by Joo and Guthrie [6]. Their computational results and experimental observation confirmed that, as the bubbles are moved off-centre, angular momenta increase, reducing mixing time considerably. It was found that a mid-radius placement of a porous plug represents an optimum location for single plug bubbling, while diametrically opposed, mid radius placement of bubblers were found to be best for dual plug bubbling. These numerical and experimental modelling exercise indicate that mixing phenomena in gas stirred ladle systems can be reasonably accurately predicted from first principles.

An alternative to the differential modelling approach to investigate mixing phenomena in gas stirred ladle systems was first applied by Sano and Mori [8]. The calculation procedure, commonly known as the circulation time model, is essentially based on the concept that the circulation time is proportional to the mixing time. Through an energy balance (e.g., at steady state, the rate of potential energy supplied by the rising bubbles is balanced by turbulence energy and interphase frictional dissipation losses), Sano and Mori derived an expression for estimating circulation time in terms of operating variables. Furthermore, by assuming mixing time to be equivalent to three times the circulation time (e.g., equivalent to a degree of mixing equal to $100 \pm 5\%$), mixing time in gas stirred cylindrical vessels containing molten iron were predicted mathematically and compared with experimental measurements. The calculated results were however, found to agree only roughly with measurements. In a later study, the same approach was also adopted by Stapurewicz and Themelis [9] to investigate mixing phenomena theoretically.

A similar approach was adopted by Krishnamurthy et al. [10] to theoretically inves-

tigate mixing phenomena in gas stirred baths. On the the basis of many experimental data derived from water model studies, Krishnamurthy et al. suggested that circulation number (= circulation time/ mixing time), in contrast to the earlier supposition of Sano and Mori [8], is not a constant and can rather assume a value between 2 and 12 (for any given degree of homogeneity). In a subsequent study, Krishnamurthy [11] applied a "tank in series model" to compute the circulation number and hence, the mixing time. Model prediction were assessed against experimental measurements and reasonable agreement claimed. However, for high temperature industrial systems agreement was found to be less satisfactory.

The models of mixing time adopted by Sano and Mori [8], Stapurewicz and Themelis [9] as well as Krishnamurthy and coworkers [10,11], are some what simplistic. Although, through tuning of some key parameters in the model equations, the circulation time models can be made to describe a particular set of experimental conditions, nevertheless, such empirical models, in general will have only limited utility, since these cannot be readily extrapolated with much confidence to other configurations. The concept applied in the formulation of the model equations are fundamentally weak since these do not incorporate the physics of the mixing process (e.g., that macro-mixing process via bulk convection, turbulent diffusion and molecular diffusion phenomena) adequately. Thus, Mietz and Oeters [1] suggested that the recirculating flow, turbulent diffusion from the tracer enriched cloud and the mass exchange between the dead zone and the remaining volume of the liquid in tanks are parameters that have to be considered in such "tank in series" or "recirculation time" models.

1.2.2   Mass transfer between solid and liquid

Thermal and mass interactions between solids and fluids are characteristics of many processes (viz., alloying addition, powder injection and so on) that are carried out in refining ladles. Over the years, several experimental studies have been reported and new empirical heat and mass transfer correlations have been developed to estimate melting and/or dissolution rates in gas stirred ladles. These investigations, in general, have appeared to

indicate that in turbulent metal processing systems, given that the intensity of turbulence is often appreciable, classical correlations for translatory flow are insufficient to connect the hydrodynamic transport phenomena to process rates. Thus, in order to estimate heat and mass transfer rates in gas stirred systems effectively, functional relationships embodying the combined influence of flow and turbulence have been proposed.

Szekely et al. [2] investigated the the dissolution rates of graphite rods dipped into industrial size gas stirred ladles. To estimate the mass transfer coefficient theoretically, the correlation proposed by Lavender et al. [12] was applied e.g.,

$$Sh = 2 + 0.72Re^{0.5}Re_t^{0.25}Sc^{0.33} \qquad (1.2)$$

A comprehensive theoretical and experimental investigation on melting phenomena in turbulent recirculatory gas bubble driven aqueous and high temperature systems has been reported by Taniguchi and co-workers [13,14]. These authors measured the melting rates of ice sphere using a photographic technique and compared them with estimates derived from three different heat transfer correlations reported in literature. Such comparisons demonstrated explicitly that the classical **Ranz-Marshall** correlation (viz., $Nu = \int +0.6(Re)^{0.5}(Pr)^{0.33}$) underpredicts heat transfer rates in gas bubble driven systems by about 40% to 50%. On the other hand, the heat transfer correlation proposed by Whitaker [15] (e.g., a modified version of the Ranz-Marshall correlation and applicable to turbulent flow situation) viz.,

$$(Nu - 2) = [0.4Re^{0.5} + 0.06Re^{0.66}]Pr^{0.4}\left(\frac{\mu_b}{mu_o}\right)^{0.25} \qquad (1.3)$$

was found to produce better estimates and was therefore more appropriate and adequate for investigating melting phenomena in both aqueous and high temperature gas stirred baths. In a later study, Szekely, Gravet and El-Kaddah [16], proposed a correlation (applicable in the range of values for Re (between 100 and 2000) and Tu (≥ 0.15)) to estimate melting rates of ice cylinders in gas bubble driven system according to:

$$Nu = 0.338(Re\ Tu)^{0.8}pr^{0.33} \qquad (1.4)$$

In order to estimate various non-dimensional numbers and hence the corresponding melting rates, a photographic technique in conjunction with a turbulent flow model was applied.

A similar approach, was adopted by Mazumdar and coworkers [17,18], for estimating mass transfer coefficients for the dissolution of benzoic acid cylinders in a gas stirred aqueous bath. On the basis of experimental measurements and numerical computations, it was demonstrated that mass transfer coefficients for vertically submerged cylinders in a water model ladle can be adequately expressed via a similar correlation of the type expressed via Eq. (1.2), e.g.,

$$Sh = 0.73 Re^{0.25} Re_t^{0.32} Sc^{0.33} \tag{1.5}$$

in which the nominal and turbulent Reynolds numbers ($Re_{loc,r}$ and Re_t) were the local flow variables and defined as ($\frac{d\rho\sqrt{u^2+v^2}}{\mu}$) and ($\frac{d\rho\bar{u}}{\mu}$), respectively. In those studies, the mean and fluctuating velocity scales embodied in the definition of nominal and turbulence Reynolds number were estimated theoretically from the $\kappa - \epsilon$ model of turbulence (e.g., $u = \sqrt{0.66\kappa}$). In a separate study, Mazumdar et al. [19] extrapolated the above equation and demonstrated that isothermal dissolution rates of steel cylinders in a carbon saturated iron melt can be predicted with reasonable certainty via Eq. (1.5). These investigations, together with many others, are therefore indicative of the fact that appropriately designed water model investigations can be reasonable and effective alternatives for studying various high temperature phenomena in ladle refining operations.

Solid and particulate dissolution rates in laboratory scale, gas stirred iron-carbon melts were reported by Wright and coworkers [20,21]. Mass transfer rates for the isothermal dissolution of steel rods were measured in two different sized (1 and 25kg) baths for a wide range of gas flow rates. It was confirmed experimentally that gas injection enhances the rate of dissolution considerably. In their subsequent study, recarburisation phenomena in a gas stirred bath were investigated via multi-particulate dissolution experiments. To compare measured and predicted particle mass transfer rates, Wright and coworkers applied the following correlation, derived from Kolmogoroff's theory of local isotropy, e.g.,

$$Sh = 2 + 0.4 \left(\frac{\epsilon d^4}{\nu^3} \right)^{0.25} Sc^{0.33} \tag{1.6}$$

It was demonstrated that Eq. (1.7) can adequately simulate multi particle dissolution phenomena (e.g., recarburisation etc.) in high temperature gas stirred system.

Asai and coworkers [22] have compiled and discussed some of the reported mass transfer correlations from the viewpoint of their applicability to ladle refining operations. One of these correlations, viz.,

$$Sh = 0.079 \, Re^{0.7} \, Sc^{0.356} \tag{1.7}$$

was subsequently applied by Koria [23] to estimate liquid velocity (e.g., Re) from the measured dissolution rates (e.g., Sh) of solid oxalic acid compacts. The fluid velocities estimated from the measured dissolution rates were compared with corresponding theoretical estimates obtained from simplified macroscopic relationships and found to be in excellent agreement. This appears to contradict the findings of many other investigations, since object Reynolds number alone has been shown to be inadequate to simulate observed heat and mass transfer rates in gas stirred ladles. Nevertheless, in view of the relatively small size of the vessel (L=0.15m and D= 0.15m)applied in conjunction with low gas flow rates, it is not unlikely that intensity of turbulence in that system was small and therefore, a correlation (essentially valid under laminar flow conditions) embodying only object Reynolds number produce reasonable estimates of dissolution rates. It is also useful to note that the intensity of turbulence within a gas stirred ladle is strongly spatially dependent. Furthermore, flows across the ladle's base and regions deep within the ladle are among the slowest. Consequently, the regions in which dissolution is measured must greatly affect the conclusions drawn.

The subsurface motions and trajectories of solid additions to gas stirred ladle systems were investigated both theoretically and experimentally by Mazumdar and Guthrie [24]. Their study suggested that under industrial conditions, buoyant additions, irrespective of their size, have practically no chance to undergo prolonged subsurface motion but rather almost instantaneously resurface. Similarly, they found that heavier additions would always sink to the bottom of the vessel. In contrast to these, neutrally buoyant additions

(e.g., some grade of ferromanganese), have the potential to undergo prolonged subsurface motion, and therefore melt within the bulk metal bath. On the basis of their physical and mathematical modelling studies, it was suggested that buoyant additions such as Al, Fe-Si, etc. would, in conjunction of variable amounts of carry-over slag, exhibit poor and erratic recovery rates, if added to ladles during argon bubbling operations. In their context, these authors highlighted the role of the C.A.S (Composition Adjustment through Sealed argon bubbling) procedure. A summary of various correlations related to heat and mass transfer have been presented in Table (1.1)

1.3   Scope of Present Work

Two phase modelling of mixing phenomena in materials processing has few and far between. In particular, combined Lagrangian-Eulerian modelling approach has not been applied so far for predicting mixing rate in gas-stirred reactors. The predictions from class of models in general depend on empirical inputs (such as, bubble diameter, drag coefficient vs Reynolds number relationship etc.) and since these are somewhat uncertain, particularly in high temperature gas stirred baths, it is important to assess the influence of these empirical parameters on the rate of predicted liquid mixing. In combined Lagrangian-Eulerian approach, the motion of gas phase is computed numerically in a Lagrangian frame of reference in the form of steady stream of bubbles while the liquid motion together with fluid turbulence is calculated by Eulerian scheme [26]. The steady state, two phase, fluid flow model in conjunction with the standard $\kappa - \epsilon$ model of turbulence is used in the present work for simulating the flow phenomena. These models are coupled with an unsteady state, species conservation equation for predicting mixing times. For mathematical analysis of mixing phenomena, it is important that predicted results are independent of grid size distribution and incremental time step. So, in the present work influence of grid size and time step on predicted mixing times has been investigated computationally.

Table 1.1: A summary of various correlations applied to investigate heat and mass transfer phenomena in metal processing operations

Correlation	Investigator	Remarks
$Sh = 0.73Re^{0.25}Re_t^{0.32}Sc^{0.33}$	Mazumdar, Khajani and Ghosh [17]	developed for analysis of dissolution phenomena in gas stirred bath
$Sh = 2 + 0.7Re^{0.5}Re_t^{0.25}Sc^{0.33}$	Szekely, Wang and Lehner [2]	for spherical geometry in turbulent shear flows
$(Nu - 2) = [0.4Re^{0.5} + 0.06Re^{0.66}] Pr^{0.4} \left(\frac{\mu_b}{mu_o}\right)^{0.25}$	Taniguchi et al. [13,14]	for spherical geometry
$Nu = 0.8(ReTu)^{0.8}Pr^{0.33}$	Szekely, Gravet and El-Kaddah [16]	for analysis of melting phenomena in turbulent gas stirred reactors
$Sh = 0.07Re^{0.7}Sc^{0.356}$	Koria [23]	for analysis of dissolution phenomena in ladle metallurgy steelmaking operations
$Sh = 0.323Re^{0.5}Sc^{0.33}$	Geiger and Poirier [25]	Forced convection over a flat plate valid for most fluid including liquid metals (Approx. Integral Technique)
$Sh = 0.646Re^{0.5}Sc^{0.33}$	do	The average mass-transfer from a flat plate to a fluid (Approx. Integral Technique)
$Sh = 0.332Re^{0.5}Sc^{0.343}$	do	The local mass-transfer for transfer from a flat plate to a fluid is given by (Exact Solution)
$Sh = 0.664Re^{0.5}Sc^{0.343}$	do	The average mass-transfer for transfer from a flat plate to a fluid is given by (Exact Solution)

Significant variations in local mixing rates in different regions of the gas-stirred vessel were reported by some investigators. In contrast some researchers have reported contradictory observations. Thus, in the present work, the position dependency of mixing in gas-stirred vessel has been analysed rigorously through mathematical model studies for different size vessels to identify the reasons for the contradictory observations. The reliability of the present model has been evaluated by comparing model predictions with experimental data. In this regard, the variation of mixing times with liquid depth has been investigated computationally.

Several mass transfer correlation have been reported (see section 2.2) in the literature which are essentially developed by curve fitting technique. These correlations are normally expressed in dimensionless form by using characteristic dimensionless groups viz., Sh, Re (local), Re (turbulent), and Sc numbers. Since, for forced convective mass transfer, Sherwood number ($\frac{Kd}{D}$) can be expressed as a function of local Reynolds number ($\frac{d(u^2+v^2)^{0.5}\rho}{\nu}$) and turbulent Reynolds number ($\frac{d\bar{u}\rho}{\nu}$), an attempt has been made in the present work to train these correlations by an artificial intelligence technique namely Genetic Adaptive Search (GAS), using the experimental and theoretical data reported in the literature so as to deduce optimal values of pre-exponent and exponents in a particular mass transfer correlation. Finally, a steady state two phase turbulent flow calculation procedure has been applied to predict mass transfer rates from first principle in two different gas stirred system and assess the adequacy and appropriateness of the GAs optimized models.

1.4 The Layout of the Thesis

The main body of the Thesis consists of five chapters. Chapter-2 deals with numerical predictions of mixing time in a gas-stirred bath. In this chapter, a steady state two phase turbulent flow model and an unsteady state, species conservation equation (that were solved for predicting mixing time) are explained. In Chapter-3, the development of mass transfer correlations by applying Genetic Algorithms has been presented. In this

chapter modelling of mass transfer from the first principle has also been briefly discussed. Chapter-4 summarises the general conclusions derived from the present work. Finally, Chapter-5 concludes this Thesis with the recommendations for future work.

Chapter 2

NUMERICAL PREDICTION OF MIXING TIME IN A GAS-STIRRED BATH

2.1 Assumptions in Modelling

A combined Lagrangian-Eulerian fluid flow model in conjunction with appropriate species conservation equation has been applied in the present work to theoretically predict mixing phenomena in gas-stirred vessels. Several assumptions and idealisation are summarised below:

(i) The presence of any overlying second phase is ignored and melt-air surface was assumed to be flat.

(ii) The melt is assumed to be isothermal.

(iii) Following axial symmetry in the present gas injection configuration, variations of flow properties along the angular direction are ignored.

(iv) Discrete mono-size bubbles are assumed to be generated at the lance tuyer/tip. Thus, the size of the bubbles created at the tip is known a-priori. The bubble frequency is calculated from the principle of volume continuity.

(v) Bubble - bubble interactions are assumed to be negligible and hence drag coefficient correlation, applicable to the single bubble-fluid system is applied to the appropriate

range of Etvos and Reynolds number.

(vi) Bubbles within the upwelling plume contribute to the generation of turbulence and this in turn affects the bubble motion.

(vii) The fluid is essentially Newtonian and incompressible and finally,

(viii) The flow is assumed to be steady, turbulent and recirculatory.

2.2   The Mathematical Model

2.2.1   Governing equation of liquid mixing

In the presence of a two - dimensional velocity field, with no generation, the conservation of mass is expressed in terms of cylindrical polar co-ordinates as

$$\frac{\delta}{\delta t}(\alpha_l \rho m_i) + \frac{\delta}{\delta z}(\alpha_l \rho u m_i) + \frac{1}{r}\frac{\delta}{\delta r}(\alpha_l \rho u r m_i) = \frac{\delta}{\delta z}(\tau \alpha_l \frac{\delta m_i}{\delta z}) + \frac{1}{r}\frac{\delta}{\delta r}(\tau \alpha_l r \frac{\delta m_i}{\delta r}) \quad (2.1)$$

Where τ, effective exchange coefficient (μ_t) can either be approximated using an effective viscosity formula proposed by Sahai and Guthrie[26], or from an appropriate turbulence model.

2.2.2   Governing equation of liquid phase motion

The knowledge of flow fields (i.e u and v) and turbulence parameter (i.e μ), are required to solve the concentration (mass) equation.

A brief outline of the combined Eulerian - Lagrangian two phase, two dimensional turbulent flow model developed earlier by Mazumdar and Guthrie[26] is presented below. The governing equations together with their boundary conditions applicable to axisymmetrical gas stirred ladles are written in terms of cylindrical co-ordinates. .

Equation of continuity

$$\frac{\delta}{\delta z}(\rho_l \alpha_l u) + \frac{1}{r}\frac{\delta}{\delta r}(\rho_l \alpha_l r v) = 0 \tag{2.2}$$

Equation of motion in the axial direction

$$\frac{\delta}{\delta z}(\alpha_l \rho_l uu) + \frac{1}{r}\frac{\delta}{\delta r}(\rho_l \alpha_l r uv) = -\alpha_l \frac{\delta p}{\delta z} + 2\frac{\delta}{\delta z}(\alpha_l \mu_e \frac{\delta u}{\delta z}) + \frac{1}{r}\frac{\delta}{\delta r}(\alpha_l \mu_e r \frac{\delta u}{\delta r}) +$$
$$\frac{1}{r}\frac{\delta}{\delta r}(\alpha_l \mu_e r \frac{\delta v}{\delta z}) + F_z \tag{2.3}$$

Equation of motion in the radial direction

$$\frac{\delta}{\delta z}(\alpha_l \rho_l uv) + \frac{1}{r}\frac{\delta}{\delta r}(\rho_l \alpha_l r vv) = -\alpha_l \frac{\delta p}{\delta r} + \frac{\delta}{\delta z}(\alpha_l \mu_e \frac{\delta v}{\delta z}) + 2\frac{1}{r}\frac{\delta}{\delta r}(\alpha_l \mu_e r \frac{\delta v}{\delta r})$$
$$+ \frac{\delta}{\delta z}(\alpha_l \mu_e \frac{\delta u}{\delta r}) + \frac{2v\mu_e \alpha_l}{r^2} + F_r \tag{2.4}$$

2.2.3 Governing equation of liquid phase turbulence

In the present work a modified form of standard coefficient $\kappa - \epsilon$ model of Launder and Spalding [27] was used. The governing equations for turbulence kinetic energy, κ and its dissipation rate, ϵ, can be represented in the cylindrical polar co-ordinates as

Equation of turbulence kinetic energy, κ

$$\frac{\delta}{\delta z}(\rho_l \alpha_l \mu \kappa) + \frac{1}{r}\frac{\delta}{\delta r}(\rho_l \alpha_l r v \kappa) = \frac{1}{r}\frac{\delta}{\delta r}(r\alpha_l \frac{\mu_T}{\sigma_k}\frac{\delta \kappa}{\delta r}) + \frac{\delta}{\delta z}(\alpha_l \frac{\mu_T}{\sigma_k}\frac{\delta \kappa}{\delta r})$$
$$+ \alpha_l (G_k - \rho_l \epsilon + P_b) \tag{2.5}$$

Equation of dissipation rate of turbulence kinetic energy, ϵ

$$\frac{\delta}{\delta z}(\rho_l \alpha_l \mu \epsilon) + \frac{1}{r}\frac{\delta}{\delta r}(\rho_l \alpha_l r v \epsilon) = \frac{1}{r}\frac{\delta}{\delta r}(r\alpha_l \frac{\mu_T}{\sigma_\epsilon}\frac{\delta \epsilon}{\delta r}) + \frac{\delta}{\delta z}(\alpha_l \frac{\mu_T}{\sigma_\epsilon}\frac{\delta \epsilon}{\delta r}) +$$
$$\alpha_l (\frac{C_1 G_k \epsilon}{\kappa} - \frac{C_2 P_l \epsilon^2}{\kappa} + \frac{P_b \epsilon}{\kappa}) \tag{2.6}$$

In Eqs(2.5) and (2.6),G_k, the volumetric rate of turbulence production, is defined as

$$G_k \doteq \mu_T \left[\left[2 \left(\frac{\delta u}{\delta z} \right)^2 + \left(\frac{\delta v}{\delta r} \right)^2 + \left(\frac{v}{r} \right)^2 \right] + \left(\frac{\delta u}{\delta r} + \frac{\delta v}{\delta z} \right)^2 \right] \qquad (2.7)$$

The eddy viscosity, μ_e, appearing in Eqs (2.3) and (2.4) is defined as

$$\mu_e = \mu_T + \mu_L \qquad (2.8)$$

Where,

$$\mu_T = \frac{C_\mu \rho_l k^2}{\epsilon} \qquad (2.9)$$

The five empirical constants of the $\kappa - \epsilon$ model viz., $C_1, C_2, C_\mu, \sigma_k,$ and σ_ϵ were assigned standard values as summarised in Table (2.1):

Table 2.1: Values of constants in the $\kappa - \epsilon$ turbulence model

Constants	C_1	C_2	σ_κ	σ_ϵ	C_D
Values	1.44	1.92	1.0	1.3	1.0

2.2.4   The equation of motion of the gas phase

The analysis of motion of the gas phase has been carried out via a Lagrangian approach, in which the trajectories of individual bubbles are stochastically determined in space by solving two simultaneous ordinary differential equation in time. The Newton's second law of motion can be represented along the two co-ordinate axis, by the following equations :

Along axial direction z

$$\left(1 + 0.5 \frac{\rho_l}{\rho_g} \right) \frac{dV_{B,z}}{dt} = -\frac{3 \mu_l C_D Re}{4 d_b^2 \rho_g} (V_{B,z} - U) + 1.5 \frac{\rho_l}{\rho_g} \left[U \frac{\delta u}{\delta z} + V \frac{\delta u}{\delta r} \right] + \left(1 - \frac{\rho_l}{\rho_g} \right) g \qquad (2.10)$$

Along the horizontal / radial direction r :

$$(1 + 0.5\frac{\rho_l}{\rho_g})\frac{dV_{B,r}}{dt} = -\frac{3\mu_l C_D Re}{4d_b^2 \rho_g}(V_{B,r} - V) + 1.5\frac{\rho_l}{\rho_g}\left[U\frac{\delta v}{\delta z} + V\frac{\delta v}{\delta r}\right] \tag{2.11}$$

The two corresponding kinematic relationships which define the trajectories of bubble's within the two dimensional flow domain are :

$$\frac{dz}{dt} = V_{B,z} \tag{2.12}$$

and,

$$\frac{dr}{dt} = V_{B,r} \tag{2.13}$$

The instantaneous drag coefficient, C_D, in the Eqs. (2.10) and (2.11) is evaluated by using an experimentally determined correlation for oblate spheroid / spherical cap bubbles, and expressed as

$$C_D = \frac{0.622}{\left[\frac{1}{E_o} + 0.235\right]} for; (500 \le Re \le 5000) \tag{2.14}$$

Furthermore, Re in Eqs. (2.10) and (2.11) is the Reynolds number, and is estimated on the basis of relative velocity vector U_r, i.e

$$Re = \rho_l d_b \left[\frac{|U_b - U_f|}{\mu_l}\right] \tag{2.15}$$

In eqs. (2.10) to (2.13), $V_{B,z}$ and $V_{B,r}$ are the instantaneous components of bubble motion in the axial and the radial directions respectively. U and V, the instantaneous component of fluid motion, are estimated by summing up the relevant mean velocity components (u and v) with the corresponding fluctuating velocity components, assuming that turbulent fluctuations are essentially isotropic and follow a Gaussian probability distribution function. For example,

$$U = u + \psi\left(\frac{2k}{3}\right)^{\frac{1}{2}} \tag{2.16}$$

Where, ψ is a normally distributed random variable and varies between -1 and 1. Thus, during the rise of bubble through the liquid, the velocity fluctuations are estimated from

(i) the predicted k field and

(ii) the random variable , ψ

The velocity fluctuations are assumed to remain constant for a time span, equivalent to the eddy life time . Furthermore, the life time of the eddy, during which a characteristic velocity fluctuation is assumed to exist, is estimated from the turbulence theory according to

$$\tau = 0.195\frac{k}{\epsilon} \tag{2.17}$$

For a scalar control volume the corresponding gas voidages can be estimated from the principle of volume continuity according to :

$$\alpha_g = \frac{\textbf{volume of gas}}{\textbf{volume of control volume}} = \frac{Q_t}{\Delta V_{cv}} \sum_{m=1}^{N} \frac{t_{rm}}{N} \tag{2.18}$$

Where, $\sum_{m=1}^{N} \frac{t_{rm}}{N}$ represents the mean residence time of N bubbles in the control volume. The sum of the residence time terms can be expressed as:

$$\sum_{m=1}^{N} \frac{t_r m}{N} = \frac{N(N+1)\Delta t}{2} \tag{2.19}$$

Hence, the gas volume fraction α_g, for a particular trajectory and specific to a control volume, can be represented as:

$$\alpha_g = \frac{Q_t(N+1)\Delta t}{2\Delta V_{c,v}} \tag{2.20}$$

Once α_g values have been determined for each of the control volumes, corresponding liquid volume fraction α_l, can be easily determined, from $\alpha_g + \alpha_l = 1.0$.

It is now well accepted that the bubbles in the two phase plume region contribute significantly to the production of turbulence. The additional turbulence produced by the bubbles can be considered to be equivalent to the shear work performed on the liquid by the bubbles and therefore, the corresponding volumetric flow rate of turbulence generation , P_b, can be represented as:

$$P_b = C_b \frac{Q_t}{N \Delta V_{cv}} \sum_{m=1}^{m=n} \int_0^{t_{r,m}} \frac{3\mu_l C_D Re}{4d_b^2} (V_B - U_f)^2 dt \qquad (2.21)$$

Where, V_B is the resultant bubble velocity and U_f is the resultant fluid velocity . C_b in eq. (2.21) is a constant and takes a value between 0 and 1. The value of C_b depends on the bubble population, bubble size etc. in the two phase plume region. The constant C_b is normally determined by trial and error.

The momentum exchange terms F_z and F_r can be evaluated by assuming that the drag force experienced by bubbles acts with equal magnitude but in opposite direction. The expression for F_z and F_r can be represented in the compact tensorial notation as:

$$F_i = \frac{Q_t}{N \Delta V_{cv}} \sum_{m=1}^{m=n} \int_0^{t_{r,m}} \frac{3\mu_l C_D Re}{4d_b^2} (V_{B,i} - U_i) dt \qquad (2.22)$$

2.2.5 The boundary condition

The boundary conditions applied to the numerical solution of the set of governing equations for species conservation, fluid flow and turbulence in axisymmetrical gas stirred ladles are as follows:

(i) At axis of symmetry :

$$r = 0; \qquad 0 < z < L; \qquad v = 0, \frac{\delta u}{\delta r} = \frac{\delta k}{\delta r} = \frac{\delta \epsilon}{\delta r} = 0 \ and \ \frac{\delta m_i}{\delta r} = 0 \qquad (2.23)$$

(ii) At the free surface of the liquid :

$$z = L; \qquad 0 < r < R; \qquad u = 0, \frac{\delta u}{\delta z} = \frac{\delta k}{\delta z} = \frac{\delta \epsilon}{\delta z} = 0 \ and \ \frac{\delta m_i}{\delta z} = 0 \qquad (2.24)$$

(iii) At the side wall :

$$r = R; \qquad 0 < z < L; \qquad u = v = k = \epsilon = 0 \ and \ \frac{\delta m_i}{\delta z} = 0 \qquad (2.25)$$

(iv) At the bottom surface :

$$z = 0; \qquad 0 \leq r \leq R; \qquad u = v = k = \epsilon = 0 \ and \ \frac{\delta m_i}{\delta r} = 0 \qquad (2.26)$$

The description of boundary conditions is shown in the Fig.(2.1).

2.3   Numerical Solution Procedure

The governing equations have mainly three terms viz., convection term, diffusion term and source term. The first order derivatives are convection terms and the second order derivatives are diffusion terms. Thus, to numerically solve the set of partial differential equations represented by equation (2.1) through (2.13) together with the boundary conditions, a control volume based finite difference [28] procedure has been adopted in the present work. In this, the flow domain has been discretized into a number of non-overlapping control volumes and the governing equations integrated around all these control volumes to result into a system of algebraic equations. The staggered control volumes have been considered for the velocity components (axial and radial velocity) and scalar control volumes for $\kappa, \epsilon, p \ and \ m_i$. The two-dimensional discretization algebraic equation can be written as:

$$a_P \Phi_P = a_E \Phi_E + a_W \Phi_W + a_N \Phi_N + a_S \Phi_S + b, \qquad (2.27)$$

in which, a_P is the centre point coefficient while a_E, a_W, a_N, a_S are the neighbour point (2 Dimensional) coefficients, representing the combined influence of fluid convection and diffusion and b is the source term. If unsteady term is present in governing equation, two terms a_P^o and Φ_P^o will come into the picture. Then,

$$a_P^o = \frac{\rho_P^o \Delta x \Delta y}{\Delta t} \qquad (2.28)$$

$$b = S_C Vol. + a_P^o \Phi_P^o \qquad (2.29)$$

Free surface of liquid

$$u = 0; \quad \frac{\delta v}{\delta z} = 0; \quad \frac{\delta \kappa}{\delta z} = 0$$

$$\frac{\delta \varepsilon}{\delta z} = 0.$$

Net mass flux = 0 at all the four surfaces.

$$\frac{\delta \varepsilon}{\delta r} = 0$$

$$\frac{\delta \kappa}{\delta r} = 0;$$

$$\frac{\delta u}{\delta r} = 0; \quad v = 0;$$

z (u)

r (v)

Axis of symmetry

$$u = 0; \quad v = 0; \quad \kappa = 0; \quad \varepsilon = 0$$

Inside wall

Wall function applied to the in the immediate vicinity of wall $r = 0$ $z = 0$

Bottom wall

Gas injection nozzle / plug
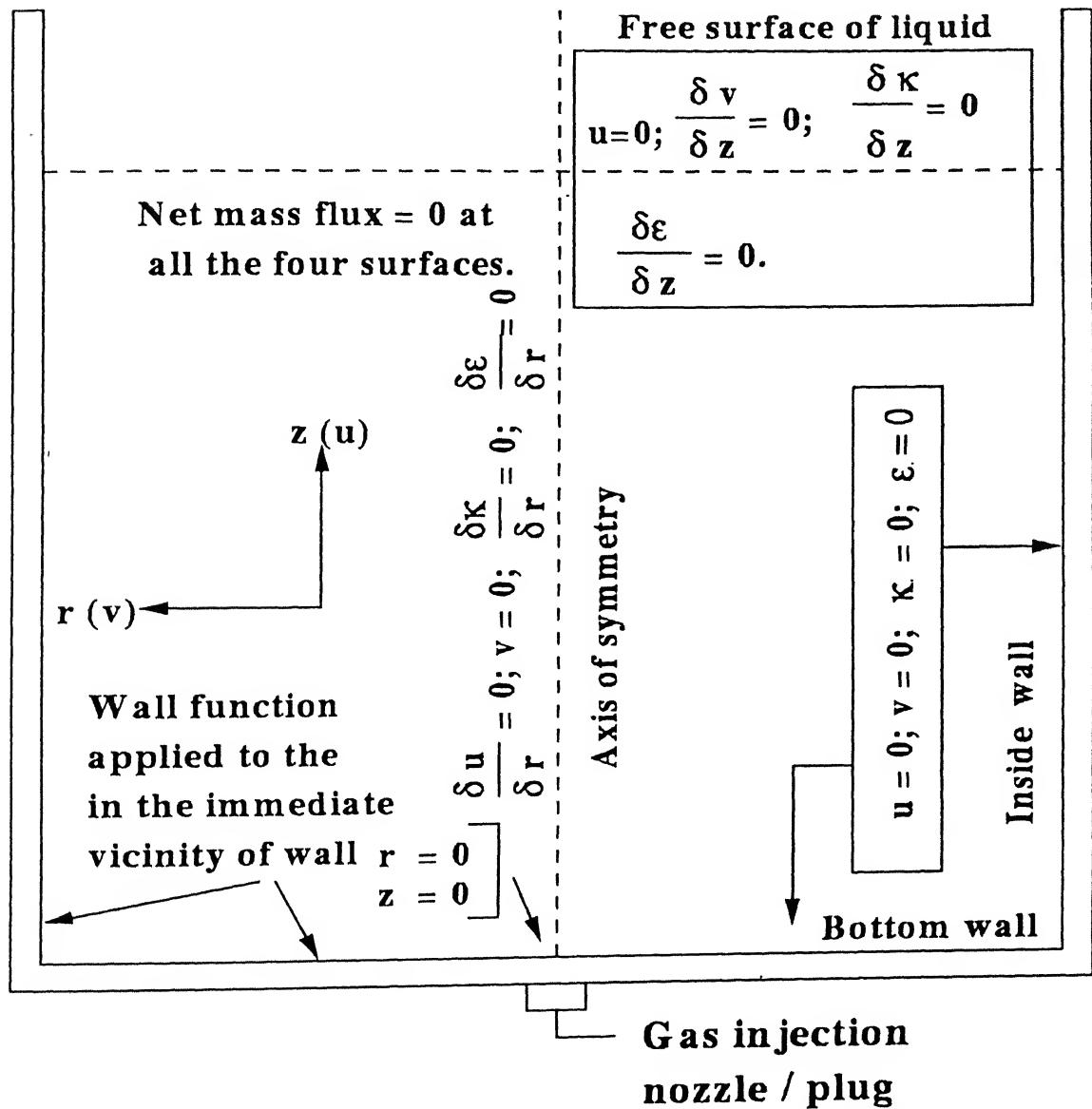
Figure 2.1: Schematic of the axi-symmetric gas-stirred bath illustrating the co-ordinate system and the boundary condition used for numerical simulation
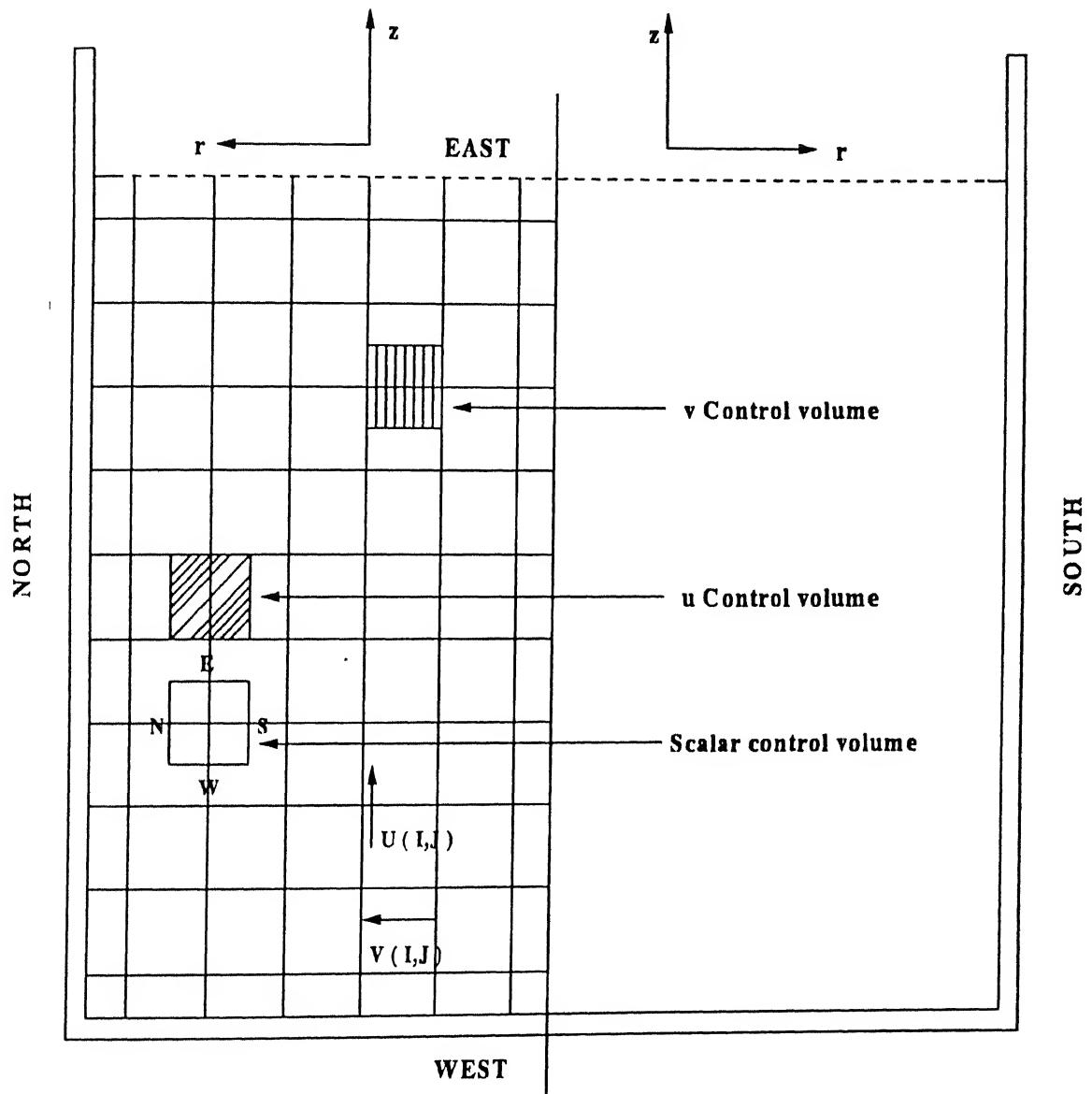
Figure 2.2: Various types of control volumes and grid distributions used in the numerical solution scheme

$$a_P = a_E + a_W + a_N + a_S + a_P^o - S_P \ Vol. \tag{2.30}$$

Here Φ_P^o and ρ_P^o refer to the known values at time t, while all other values (Φ_P, Φ_N, and so on) are the unknown values at time $t + \Delta t$. For steady state governing equation the value of a_P^o will become zero. Further, S_C represents the positive component of the linearised source term, while the corresponding slope is included in the a_P term. The set of algebraic equations thus derived has been solved via the Tri-diagonal Matrix Algorithm(TDMA), through a line by line solution technique. The pressure-velocity interlinkage in equations (2.2) through (2.6) has been solved by an implicit finite difference procedure known as SIMPLE [28] (Semi-Implicit method for pressure linked Equations). Since an iterative calculation procedure has been adopted to numerically solve the governing partial differential equations, a convergence criteria has been prescribed. To this end a residual source has been defined as:

$$Residual\ source = \left(\sum a_{nb}\Phi_{nb} + S_C - a_P\Phi_P\right) \qquad \leq 10^{-3} \quad (SI\,unit) \tag{2.31}$$

In which, a_{nb} is the neighbouring point value. The modulus of this residual source has been estimated at each nodal point and added up over the entire flow domain for each individual variable involved. The steps involved for the prediction of mixing time are:

(i) Velocity field (u, v) and effective viscosity (μ_e) were calculated from flow and turbulence models .

(ii)By using u, v and μ_e, normalized concentration profiles f(z,r,t) were obtained. Normalized concentration is expressed as:

$Normalized\ concentration = \frac{Local\ concentration}{Bulk\ concentration}$

Average or bulk concentration was calculated by using the following relationship:

$$\bar{C}_b = \frac{\int_0^R \int_0^L m_i (2\pi r) dr dz}{\int_0^R \int_0^L (2\pi r) dr dz} \tag{2.32}$$

In other form,

$$\bar{C}_b = \frac{\sum \sum m_i \times VOL(I,J)}{\sum \sum VOL(I,J)} \tag{2.33}$$

(iii)Normalized concentration profiles (i.e. dimensionless concentration vs. time plots) were obtained in the different regions of the vessel. This provides the idea of the rate of mixing at various locations in the vessel. The flow circuit of the computer program applied to the present study has been illustrated in Fig. (2.2).

```
                    ( START )
                        |
        +-----------------------------------+
        | Establish main grid, specify flow |
        | properties, turbulence model      |
        | constant etc.                     |
        +-----------------------------------+
                        |
        +-----------------------------------+
        | Establish staggered grid, calculate|
        | all geometrical quantities and    |
        | initializes all variables         |
        |      ( u, v, p, K, ε )            |
        +-----------------------------------+
                        |
        +-----------------------------------+
        | Establish bubble trajectories and |
        | update                            |
        +-----------------------------------+
                        |
        +-----------------------------------+         +-------------------------+
        | Calculation of axial velocity     |         | Define Exchange coefficient |
        |            component              |         +-------------------------+
        +-----------------------------------+                      |
                        |                             +-------------------------+
        +-----------------------------------+         | Time = Time + timestep  |
        | Calculation of radial velocity    |         +-------------------------+
        |            component              |                      |
        +-----------------------------------+         +---------------------------------+
                        |                             | Calculation of dimensionless concentration |
        +-----------------------------------+         +---------------------------------+
        | Calculation of pressure           |                      |
        +-----------------------------------+                   /  Is  \
                        |                         NO          / Convergence criteria \
        +-----------------------------------+     <--------   \   satisfied   /
        | Calculation of turbulence energy  |                   \       /
        +-----------------------------------+                     |YES
                        |                         Less than maximum time  +------+
        +-----------------------------------+     <----------------------| TIME |
        | Calculation of energy dissipation |                            +------+
        +-----------------------------------+                      Greater than
                        |                                          Maximum time
        +-----------------------------------+                        +-------+
        | Estimates turbulence viscosity    |                        | PRINT |
        +-----------------------------------+                        +-------+
                        |                                               |
                     /  Is  \                                        ( STOP )
        NO         / Convergence criteria \
        <-------   \   satisfied ?   /
                     \       /
                        |
                       YES
```

Figure 2.3: Flow chart of computer model used in the present study

2.4 Results and Discussion

2.4.1 The spatial dependency of mixing : the definition of bulk mixing time

The mixing phenomena in a gas stirred bath is related to the turbulent recirculatory fluid motion developed due to injection of gas. Since the flow and turbulence are spatially dependent, it is important to study the variation of mixing rates in different regions of the vessel. Normalised concentration profiles have been plotted in Fig. (2.4), as a function of time for three different regions (A, B and C) of the gas stirred vessel (L=0.80m and R= 0.56m). The rate of mixing and thus mixing times are different for different regions of the vessel. Thus, to quantify a reactor mixing time, a 95% bulk mixing time criterion has been applied. This is defined as the time by which the vessels content at every location is at least 1 ± 0.05 of the equilibrium concentration. Obviously then, 95% bulk mixing time is equivalent to the 95% local mixing time of the slowest mixing region/location. Table (2.2) represents the values of mixing time at three regions of for a axisymmetric gas stirred vessel. The region A, which is bottom corner portion of a vessel has maximum value of mixing time. In this region species reach at last so this region is considered for the evaluation of mixing time. The region B is the central while C is the upper corner location of the vessel. It is seen that region B and C have less value of mixing time than that of A. As seen, from Table (2.2) and Fig.(2.4), significant variation in local rates of

Table 2.2: Values of numerically predicted mixing times at different locations of a gas stirred bath

SL. No.	Location, (r,z)cm	Mixing time (second)	Region region
1	(52.5,1.43)	78	A
2	(52.5,4.29)	70	A
3	(26.8,38.6)	59	B
4	(54.8,78.5)	63	C

mixing is observed for different regions of vessel. It is found that region A close to the
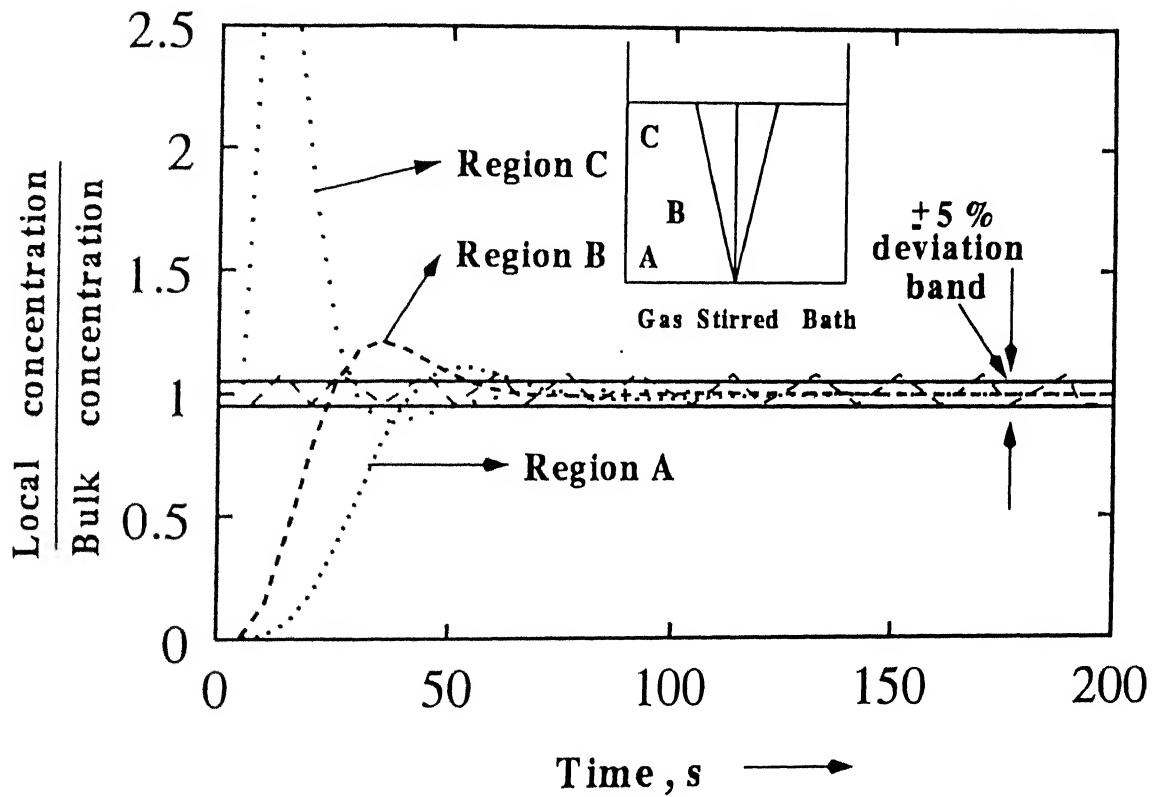
Figure 2.4: Variation in local mixing time for three different regions, A, B and C in a gas stirred vessel (grid Size $= 30 \times 26$, L $= 0.8$m, R $= 0.56$m, $d_b = 0.015$m, gas flow rate $= 6.67 \times 10^{-4}$ m^3/s and $C_b = 0.0$)

bottom of the ladle exhibited the slowest rate of mixing. Hence, it is clear from numerical predictions that by the time region A approached the 95 percent mixing mark, the bulk of the liquid was practically homogeneous. Thus, region A is better representative of the bulk 95 percent mixing time of the system than those of locations B and C.

2.4.2 Influence of grid size distribution on predicted mixing time

The solutions of the governing differential equations for the prediction of mixing time are expected to be sensitive to the nodal configuration applied to the numerical solution scheme. It is therefore essential to obtain grid independent solutions prior to analysis of various aspects on mixing time (viz., influence of time step, location ,bubble diameter etc).

To test these, mixing times (via concentration profiles) in a gas stirred cylindrical vessel (L=0.80m and R=0.56m) have been predicted by applying four different grid configurations viz., 35×30, 30×26, 28×20 and 20×17, along z and r, respectively. In each case, the location of prediction has been kept nearly the same. A comparison of numerically predicted concentration profiles of different grid distribution is shown in fig.(2.5). The values of the corresponding predicted mixing time for different grid system, as summarised in table (2.3), indicates that both 30×26 and 28×20 grid systems give almost same value of mixing time. Consequently, to be on the safer side, numerical predictions via a 30×26 grid system is considered to be essentially grid independent.

2.4.3 Influence of incremental step size on predicted mixing time

In earlier sections, the unsteady liquid mixing equation has been coupled with steady fluid flow and turbulence equations to predict the mixing time in a gas stirred bath. However, due to two dimensional nature of the transient mass conservation equation, an iterative

Table 2.3: Predicted variation of mixing time as a function of grid size distribution.

SL. No.	Grid Size	mixing time (second)	Location (r,z)cm
1	30×26	69sec	(54.8,1.43)
2	35×30	77sec	(53.0,3.63)
3	28×20	69sec	(54.4,1.53)
4	20×17	152sec	(54.1,2.22)
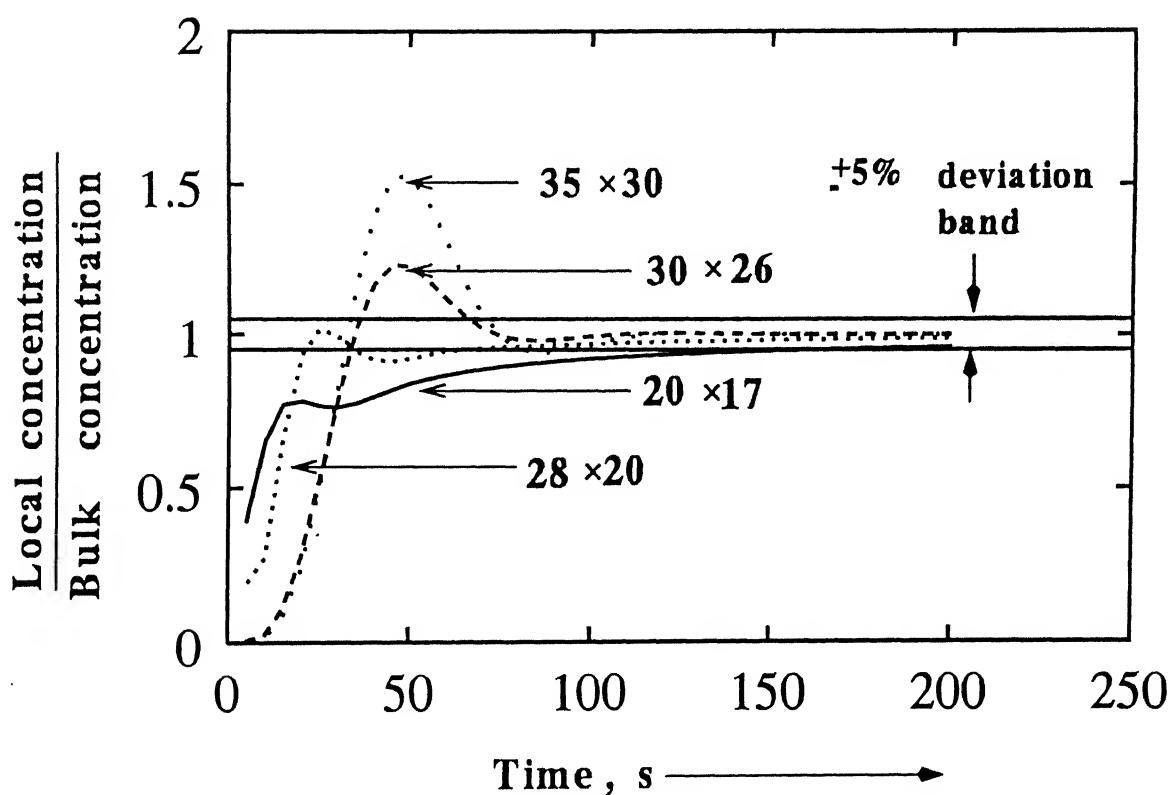
Figure 2.5: Variation in predicted mixing time as a function of grid size distributions ($\Delta t = 5$sec, L = 0.8m, d_b = 0.015m, gas flow rate = 6.67×10^{-4} m^3/s, and C_b = 0.0)

scheme has to be employed to obtain the normalized concentration profile numerically. The discretisation equation of the unsteady mass conservation equation includes time step (Δt) term (Eq. 2.24). Like grid size distribution, numerical predictions are also sensitive to time step. Hence, it is also important to establish solutions independent of the time step for further analysis. For this, normalized concentration profiles in a axisymmetric gas stirred cylindrical vessel (L=0.80m and R=0.56m) have been predicted numerically by applying four different time steps viz., 3.5, 5, 10 and 20 seconds respectively. All other parameters were, kept fixed. Figure (2.6) represents the normalised concentration profiles for different time step values. The corresponding values of predicted 95% bulk mixing time for different time step (at the same location in all cases) have been presented in Table (2.4). It is clear from Table (2.4) that both 3.5 and 5 seconds produce same values mixing time. Hence on the basis of above analysis, 5 second is considered as a reasonable value of time step (Δt) for numerical simulation.

Table 2.4: Predicted variation of mixing time as a function of different time step at a particular location of a gas-stirred bath

SL. No.	Time step (second)	Mixing time (second)	Location (r,z)cm
1	3.5	73sec	(52.5,1.43)
2	5.0	73sec	(52.5,1.43)
3	10.0	93sec	(52.5,1.43)
4	20.0	139sec	(52.5,1.43)

2.4.4   Comparison with experimental results

To assess the predictive capability of the mixing time model, normalized concentration profiles in gas stirred bath for different liquid depths viz., 0.5, 0.6, 0.8, 0.93 and 1.0 meter for a fixed vessel radius = 0.56m have been predicted numerically and from these profiles, 95% bulk mixing times were calculated for each configuration. Due precaution was taken so that the predicted mixing time truly reflects the bulk mixing time. Table (2.5) shows the value of the mixing time as function of liquid depth in the vessel. This indicates that
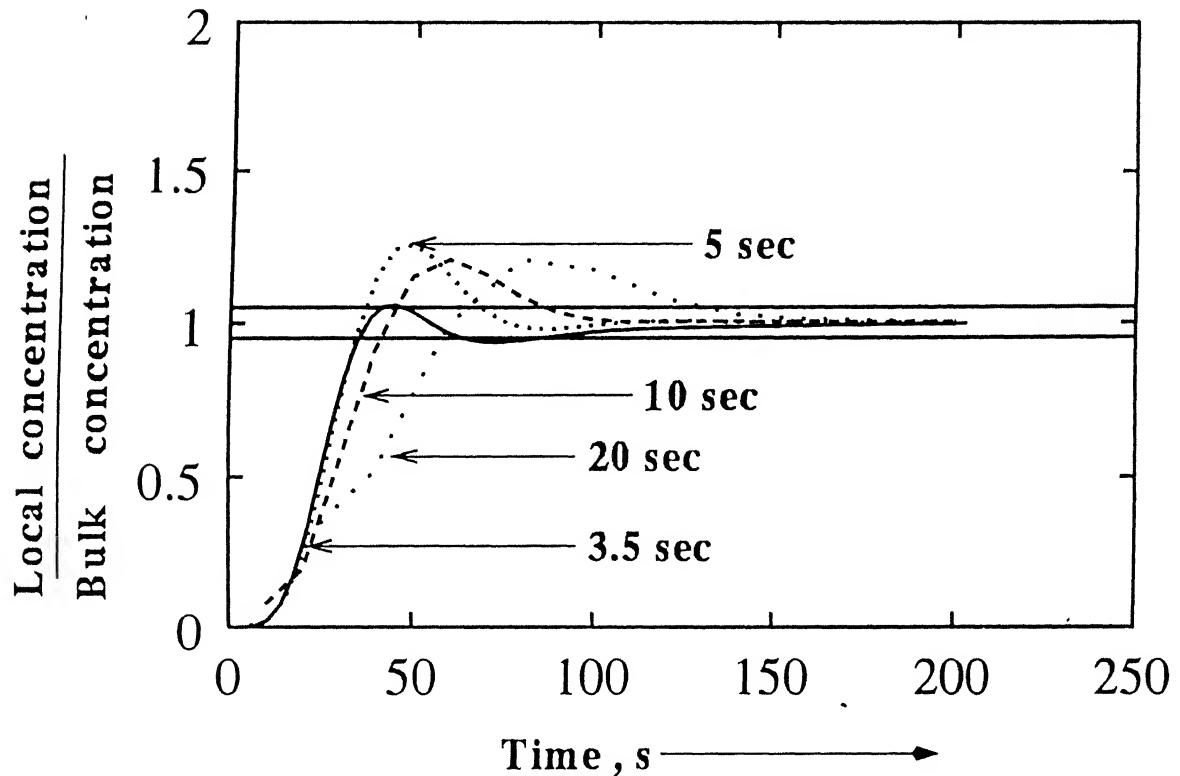
Figure 2.6: Variation in predicted mixing time as a function of four different incremental time steps (3.5, 5, 10 and 20 seconds), illustrates the specific value of Δt for time step independent numerical prediction (grid Size $= 30 \times 26$, L $= 0.8$m, R $=0.56$m, $d_b = 0.015$m, gas flow rate $= 6.67 \times 10^{-4}$ m^3/s, $C_b = 0.0$)

mixing time decreases as depth of liquid increases. This is expected because the potential energy input rate of the system is directly proportional to the to the depth of liquid. In Fig.(2.7) the theoretically predicted mixing time has been plotted as a function of liquid depth and compared directly with experimental measurement of Mazumdar and Guthrie [5]. Reasonable agreement between prediction and measurement is readily apparent.

Table 2.5: Predicted variation of mixing time as a function of liquid depth of a gas-stirred bath

SL. No.	Bath height (meter)	Mixing time (second)	Location (r,z)cm
1	0.5	93	(52.5,4.5))
2	0.6	80	(52.5,5.3)
3	0.8	71	(52.5,4.3)
4	0.93	48	(52.5,4.98)
5	1.00	43	(52.5,5.35)

2.4.5 Influence of empirical model parameters on predicted mixing time

The interphase friction forces $(F_z and F_r)$ and the turbulence production (P_b) due to bubbles (Eq. (2.21) and Eq. (2.22)), are dependent on parameters such as bubble diameter (d_b), turbulence production constant (C_b) etc. The turbulence constant (C_b) takes a value between 0 and 1, and this is a function of bubble population, shape and size etc. It is obvious that the values of these parameters applied in the numerical solution scheme would affect the mixing time. While in earlier calculations the mean experimental value of bubble diameter was applied, additional calculations were carried out by considering different bubble diameters to assess the sensitivity of predicted results to d_b. Thus a new bubble diameter has been calculated by applying following expression [29]:

$$d_b = 0.35 \left(\frac{Q^2}{g} \right)^{0.2} \tag{2.34}$$
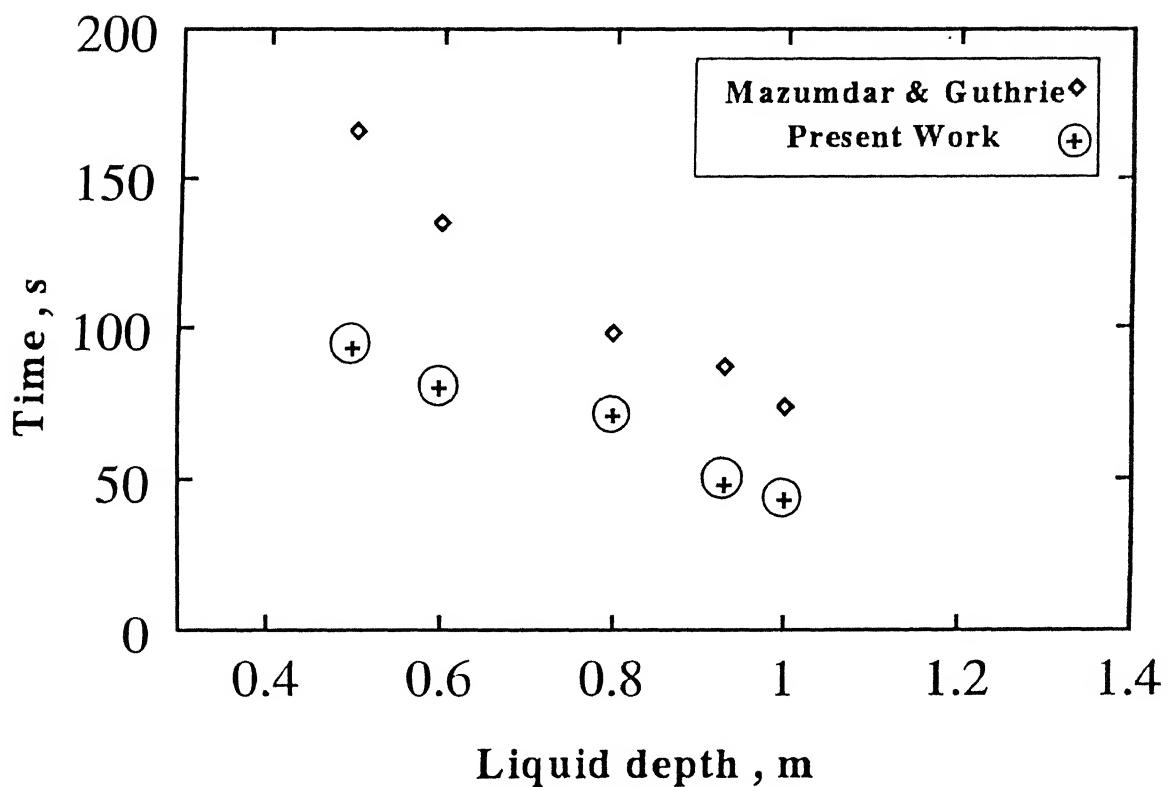
Figure 2.7: Theoretically predicted mixing times as a function of liquid depth for a gas-stirred vessel for(grid Size = 30 × 26, R = 0.56m, d_b = 0.015m, gas flow rate = 6.67×10^{-4} m^3/s, C_b = 0.0) and their comparison with experimental results.

Where;

Q = Gas flow rate.

g = Acceleration due to gravity.

The value of d_b calculated from above equation is approximately 0.01 m. In the subsection 2.4.4, theoretical prediction of mixing times were carried out for $d_b = 0.015$ (experimental value). Table (2.6) represents the values of mixing time for five bath depths viz., 0.5, 0.6, 0.8, 0.93 and 1.0m, deduced for a d_b value of 0.01m. This shows that, predicted mixing time for d_b =0.01m is more close to the observation of Mazumdar and Guthrie[5] than that of $d_b = 0.015m$. It is to be emphasized that the exact value of bubble diameter used in the numerical solution scheme is likely to influence the predicted results to some extent.

Subsequent to this, influence of C_b values on predicted mixing time has been analysed. Mixing times were predicted numerically for two different value of C_b viz., 0.5 and 0.7 and compared with experimentally measured results[5]. The comparison shows (Fig. (2.9)) that predicted mixing time is sensitive to the previous values of the empirical constant C_b.

Table 2.6: Predicted estimates of mixing time for theoretically deduced bubble diameter value of 10mm.

SL. No.	Bath height (meter)	Mixing time (second)	Location (r,z)cm
1	0.5	100	(52.5,4.5))
2	0.6	87	(52.5,5.3)
3	0.8	78	(52.5,4.3)
4	0.93	61	(52.5,4.98)
5	1.00	56	(52.5,5.35)
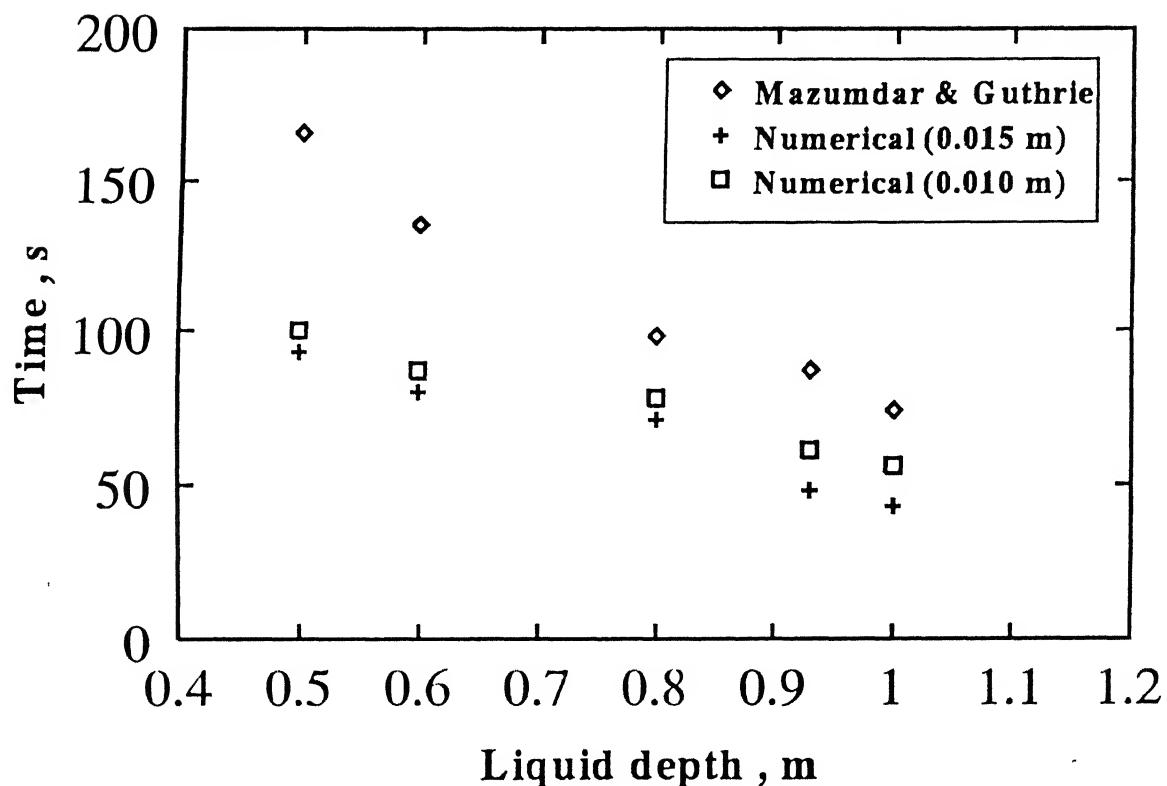
Figure 2.8: Theoretically predicted mixing times as a function of liquid depth, for different bubble diameters (0.015 m and 0.01m) and their comparison with experimental observations)
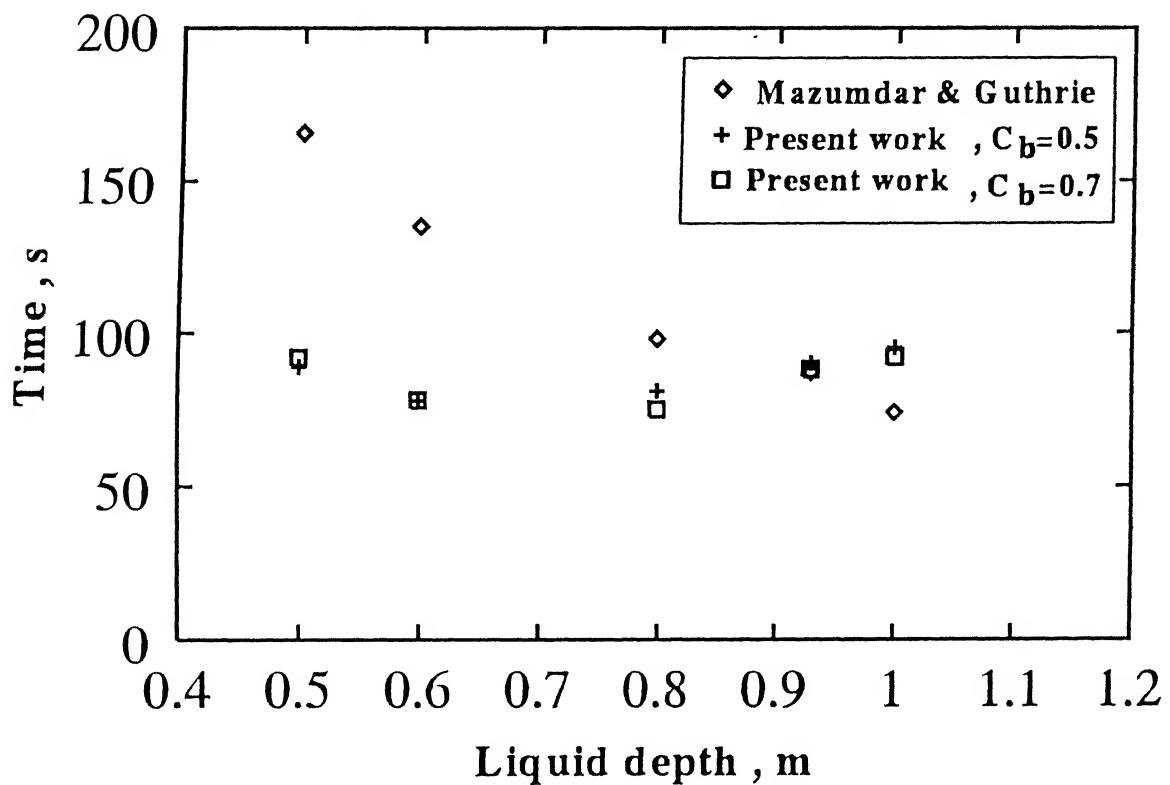
Figure 2.9: Theoretically measured mixing time as a function of liquid depth for different values of turbulence production constant ($C_b = 0.5 and 0.7$) and their comparison with experimental results.

2.4.6 The spatial dependency of mixing: the influence of scale factor (the size of the vessel)

As pointed out previously, some investigators have reported on the variation of mixing times at different locations in the vessel, while others have reported contradictory observations. An analysis of these investigations show that vessel size as well as degree of mixing were different in the studies. Consequently, mixing time was predicted in a smaller size vessel (L=0.24m and R=0.35m) to primarily assess the influence of 'scale factor' on the rate of mixing at various locations. In Fig. (2.10) variation of mixing rates in three different regions of the vessel are shown. The nature of the curves for respective regions are essentially identical to those already shown for a bigger size vessel under identical operating gas flow rates. In Figure (2.11), local mixing times for the three regions have been plotted as a function of degree of mixing (varied arbitrarily between 90 to 99%)for the two different vessels. It is observed that

(i)the magnitude of difference between the mixing times at various locations tend to diminish as the degree of mixing is made more stringent.

(ii)Smaller the vessel size, smaller is the difference between local mixing times for any degree of mixing.

This indicates that position dependency of mixing is not universal and is a function of vessel size and the criterion of mixing applied.
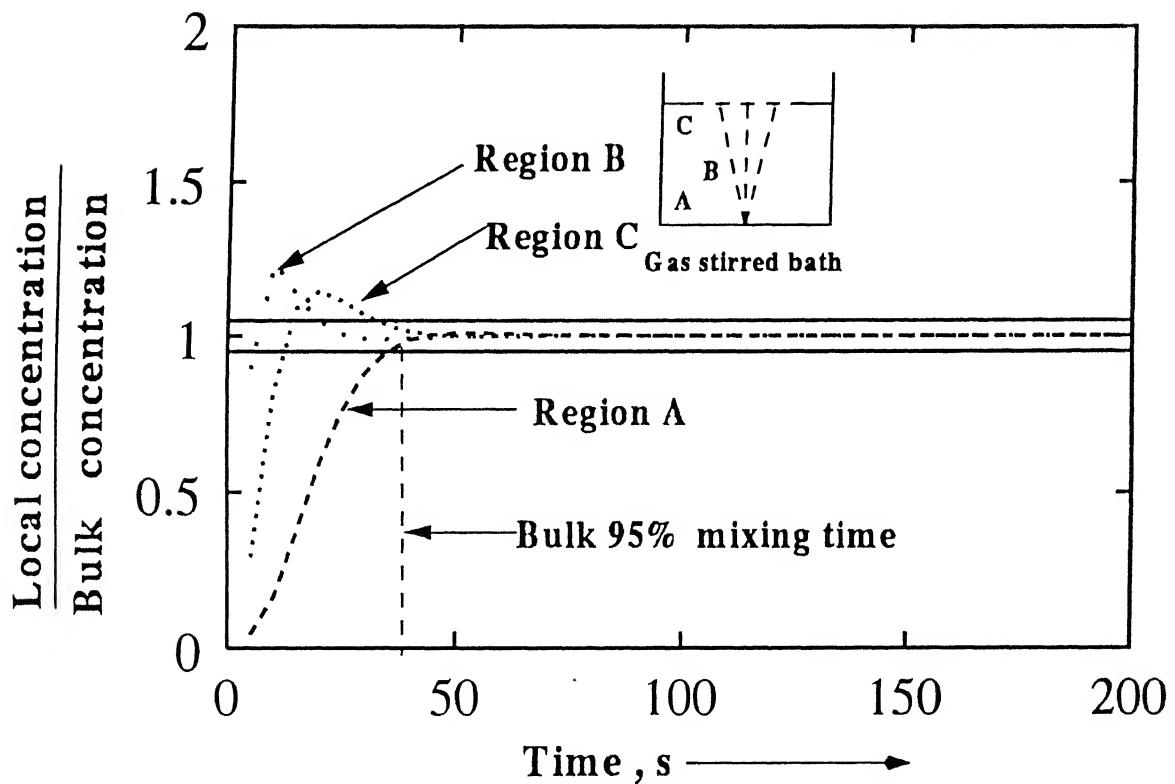
Figure 2.10: Variation in local mixing time for three different regions, A, B and C in a small gas stirred vessel (grid Size = 12 × 18, L = 0.24m, R = 0.35m, d_b = 0.015m, gas flow rate = 6.67×10^{-4} m^3/s and C_b = 0.0)
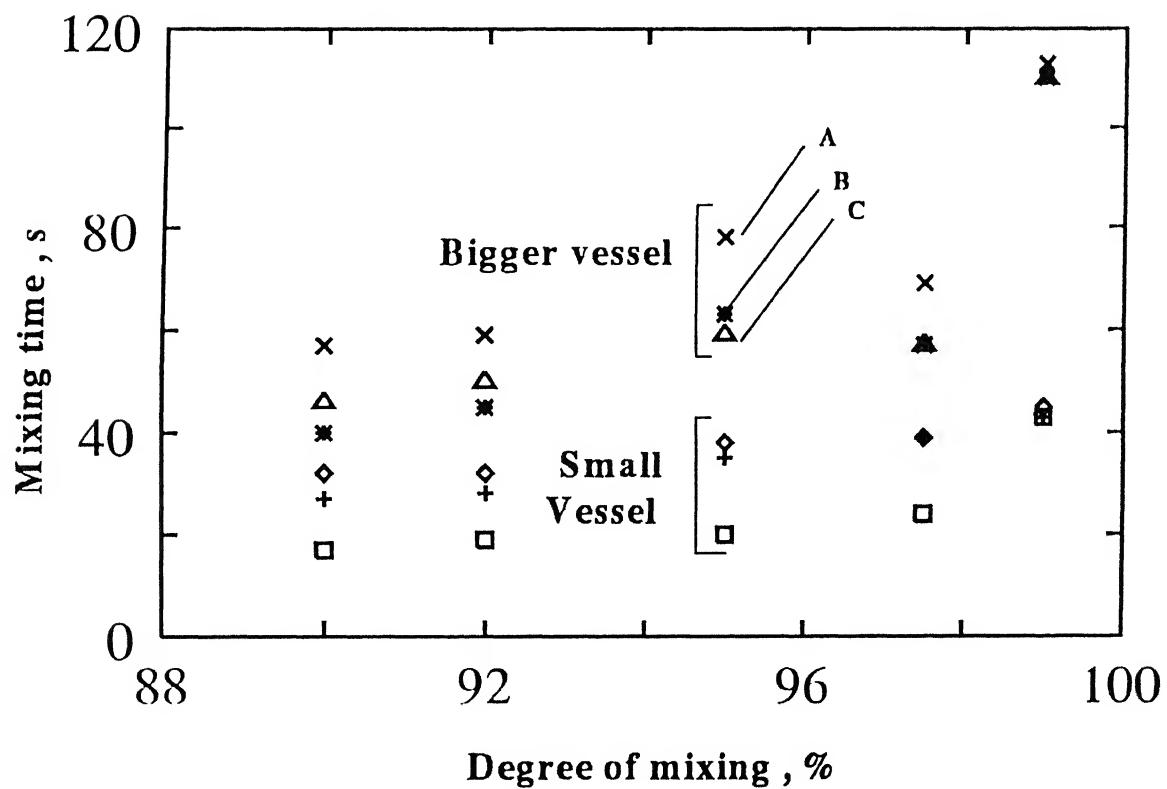
Figure 2.11: Effect of degree of mixing (viz., 90%, 92%, 95%, 97.5% and 99%) on local mixing times in different type of gas stirred vessels

Chapter 3

PREDICTION OF MASS TRANSFER RATES BETWEEN SOLID AND LIQUID IN GAS STIRRED BATH

3.1 The General Method of Prediction of Solid-Liquid Mass Transfer Rates

Numerous mass transfer correlations have been developed for forced convective mass transfer situation embodying three key dimensionless numbers viz., Sh, Re, Sc. These mass transfer correlations generally assume a functional form of the type:

$Sh = f(Re, Sc, geometry)$

Using such correlations, mass transfer rates between solid-liquid can be predicted either from a purely experimental or a combined experimental and theoretical stand point. In case of mass transfer from a solid sphere or cylinder, the Sherwood number (Sh) is related to dissolution rate ($\frac{dR}{dt}$) while Reynolds numbers is related to the flow characteristics. Under the turbulent flow conditions, contribution to mass transfer arises from nominal Reynolds number as well as turbulent Reynolds number. Mass transfer rates in an axisymmetric gas stirred bath therefore can be predicted via any available correlation, using measured flow fields or can be directly obtained by monitoring the dissolution rate

experimentally.

3.2   Methodology of Developing a Mass Transfer Correlation

Most of the mass transfer correlations have been developed by curve-fitting to experimental data. Various techniques can be adopted to develop mass transfer correlations, include viz., curve-fitting (linear or multiple regression) to a set of experimental measurements, curve-fitting to a set of data derived partly experimentation and partly through theoretical analysis, dimensional analysis, approximate integral technique, exact solution technique, etc. In addition to the above, modern artificial intelligence techniques such as, GAs and Artificial Neural nets (ANN) can also applied to a given same set of data to optimize the functional form of a given correlation. In this chapter possible application of GAs is examined from the view point of obtaining a mass transfer correlations with optimal pre-exponent and exponents.

3.3   Possible Application of Genetic Algorithms for Correlation Development

GAs are robust search and optimization techniques and are applicable to solve complex, multimodal, discrete or discontinuous problems. The details of technique are provided elsewhere [30,31,32]. Flow diagram of (SGA) code used in present work is provided in Fig.3.1.
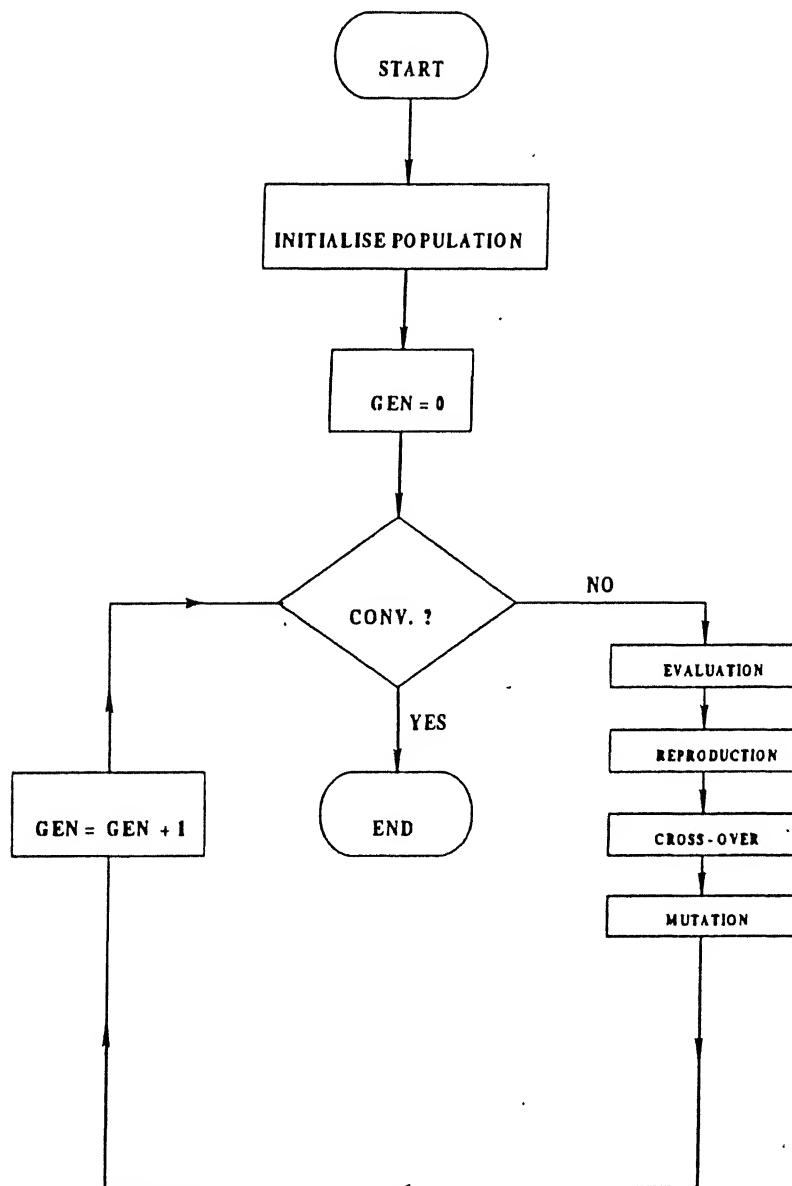
Figure 3.1: Flow diagram for the Simple Genetic Algorithm (SGA) code used in the present study [31]

3.4 Derivation of Correlation from a Set of Data via GAs

Experimental data of Singh and Mazumdar [33] and combined theoretical and experimental data of Mazumdar and coworkers [17] on dissolution of vertical solid cylinders in an aqueous model of gas stirred ladle has been considered for developing the correlations. Mazumdar [18], has shown that mass transfer rates from vertical cylinders in gas agitated reactors can be adequately described via a relationship of the type:

$$Sh = 0.73 Re_{loc,r}^{0.25} Re_t^{0.32} Sc^{0.33} \tag{3.1}$$

In the preceding equation,

Sh = Sherwood number. $\left(\frac{Kd}{D}\right)$

$Re_{loc,r}$ = Nominal local Reynolds number. $\left(\frac{d\rho(u^2+v^2)^{0.5}}{\mu}\right)$

Re_t = Turbulent Reynolds number. $\left(\frac{du\bar{\rho}}{mu}\right)$

It is important to mention here that above correlation was obtained by multiple linear regression analysis of the measured data on dissolution. This equation for the experimental configuration of Mazumdar (Sc=500) can also be represented as:

$$Sh = 5.78 Re_{loc,r}^{0.25} Re_t^{0.32} \tag{3.2}$$

In the most general form, eq.(3.2) can be written as:

$$Sh = K_1\ Re_{loc,r}^{K_2}\ Re_t^{K_3} \tag{3.3}$$

Where, K_1 is the pre-exponent term and K_2, K_3 are the exponent terms. The purpose is to determine K_1, K_2 and K_3 through a fresh analysis (by the application of GA) of the reported data. The objective function for minimization is the sum of the residual squares,

e.g.,

$$\sum_{i=1}^{n}\left((Sh)_i - \left(K_1\left(Re_{Loc}^{K_2}\right)_i\left(Re_t^{K_3}\right)_i\right)\right)^2 \tag{3.4}$$

where,

n is the total number of data points. The set of data are presented in Table(3.2) and Table(3.3) respectively.

The numerical value of various GA parameters used in the present investigation are

- $P_s = 40$

- $P_{cr} = 0.95$

- $P_m = 0.01$

- Number of generations $= 100$

- Total string length (l) $=20$, (First variable $= 8$, second variable$=6$ and third variable $= 6$)

- Appropriate range of variables, is shown in Table(3.1), the range has been selected by considering the large number of correlations reported in standard texts and relevant literature.

Table 3.1: Values of variable bounds applied in GAs correlation prediction

SL.NO.	variables	lower value	upper value
1	K_1	0.3	7.0
2	K_2	0.2	0.8
3	K_3	0.25	0.8

3.4.1   Determination of K_1, K_2 and K_3 on the basis of experimental data only

Optimal solution is obtained considering experimental data only. Total number of data (n) is 32. This is shown in Table 3.2. After first generation the optimal mass transfer

correlation obtained by GAs is:

$$Sh = 6.264 \ Re_{loc,r}^{0.23} \ Re_t^{0.35} \tag{3.5}$$

Where, pre-exponent term $= K_1 = 6.264$, and exponent terms are:

$K_2 = 0.23$, $K_3 = 0.35$

Hence, for Sc = 500, the above equation can be rewritten as:

$$Sh = 0.80 \ Re_{loc,r}^{0.23} \ Re_t^{0.35} \ Sc^{0.33} \tag{3.6}$$

3.4.2   Determination of K_1, K_2 and K_3 on the basis of theoretical and experimental data

Optimal solution in this case is obtained by considering a set of combined experimental and theoretical data. Total number of data used (Table 3.3) is 56. The optimal mass transfer correlation by GA after first generation is

$$Sh = 6.553 \ Re_{loc,r}^{0.22} \ Re_t^{0.34} \tag{3.7}$$

Where the pre-exponent term K_1 is found to be 6.553, and exponent terms are respectively $K_2 = 0.22$, and $K_3 = 0.34$. Hence, for Sc = 500, Equation (3.7) can also be written as:

$$Sh = 0.84 \ Re_{loc,r}^{0.22} \ Re_t^{0.34} \ Sc^{0.33} \tag{3.8}$$

It is interesting to note from the above that regardless of the nature of data (whether experimental or theoretical) applied to GAs, correlation is practically identical results (see Eqs. (3.5) and (3.7)). This essentially indicates that the theoretical data which were obtained through the numerical solution of the turbulent Navier-Stokes equations, match well with experimental data. This implicitly indicates that mass transfer rates can be predicted from first principles with reasonable certainty. Since the GA based

Table 3.2: The set of experimental data of dimensionless numbers [33] considered for developing a mass transfer correlation by Genetic Algorithm.

SL.NO.	Sh	Re_L	Re_t
1	170.8	419.45	93.9568
2	164.4	424.40	95.0656
3	160.6	429.05	96.1072
4	172.6	440.51	126.0846
5	177.6	447.48	128.0772
6	182.4	453.99	129.9402
7	160.28	356.384	128.871
8	170.4	360.774	130.4586
9	166.2	365.12	132.03
10	156.8	529.587	118.827
11	157.5	537.529	120.609
12	161.4	545.53	122.40396
13	156.60	626.19	163.0524
14	153.16	570.596	148.5764
15	154.4	575.939	149.9676
16	167.8	689.068	162.516
17	160.0	673.651	158.88
18	151.2	680.435	160.48
19	163.94	466.554	164.86
20	149.74	449.63	158.88
21	146.6	453.705	160.32
22	147.2	754.3	150.86
23	159.6	792.6	158.52
24	150.98	800.36	160.072
25	143.6	660.346	161.06
26	146.32	666.004	162.44
27	146.4	944.809	162.06
28	154.10	953.438	163.54
29	135.4	685.608	173.019
30	138.90	691.374	174.4742
31	145.0	808.05	161.61
32	143.08	815.5	163.1

correlations are identical to the original correlation of Mazumdar, multiple regression is equally suitable for this class of problem.

Table 3.3: Theoretically estimated data [17] of dimensionless numbers applied to develop a mass transfer correlation by Genetic Algorithm

SL.NO.	Sh	Re_L	Re_t
1	112.70	328.0	212.0
2	131.65	504.0	226.0
3	283.9	1281.0	989.0
4	140.0	186.0	130.0
5	136.1	396.0	232.0
6	162.2	617.0	287.0
7	322.05	1002.0	984.0
8	184.80	137.0	260.0
9	170.0	297.0	252.0
10	221.8	844.0	261.0
11	285.95	1172.0	723.0
12	204.9	155.0	227.5
13	151.8	596.0	200.0
14	141.95	819.0	113.0
15	328.2	2101.0	586.0
16	187.0	488.0	270.0
17	143.8	798.0	267.7
18	152.08	634.0	140.0
19	304.5	2791.0	630.0
20	186.05	647.0	356.0
21	151.3	948.0	330.0
22	178.8	763.0	170.0
23	355.2	3229.0	748.0
24	243.7	774.0	453.0

3.5 Predictions of Mass Transfer Rates Through Numerical Solution of Turbulent Navier-Stokes Equations

The distribution of flow variables (u and v) and turbulence parameters ($\kappa, \epsilon, \bar{u}$ etc.) in axisymmetric gas stirred cylindrical vessels (see Table (3.4)) have been predicted theoretically by the solution of turbulent Navier-Stokes equations in conjunction with the $\kappa - \epsilon$ turbulence model so as to predict the solid-liquid mass transfer rates. The governing equations together with the set of boundary conditions and the numerical solution procedure have already been explained in Chapter 2. The velocity components and turbulence kinetic energy in two different size vessels (see Table 3.4) were predicted. From the predicted distribution the nominal Reynolds number and the turbulent Reynolds numbers were estimated for those locations where the solid samples were kept submerged. To

Table 3.4: Experimental conditions used for computation of mass transfer rates through numerical solution of of turbulent Navier-Stokes equation.

Case	Bath Depth	Bath Radius	Gas Flow Rate	d_b	C_b	grid Size
Vessel:1	0.21m	0.15m	1 l/min	0.01m	0.7	10×8 15×10 20×16
Vessel:2	0.42m	0.238m	8 l/min	0.015m	0.7	24×20 20×16 15×10

Table 3.5: Summary of thermophysical properties employed in the present work.

Diffusivity of benzoic acid in water m^2/s	2.0×10^{-9}
Density of water, kg/m^3	1.0×10^3
Viscosity of water, $kg/m.s$	1.0×10^{-3}

this end, the resultant mean velocity components, $\sqrt{u^2 + v^2}$ were embodied in the ex-

pression of nominal Reynolds number while the isotropic fluctuating velocity components calculated from $\bar{u} = \frac{2\kappa}{3}^{0.5}$, were used in the expression of turbulent Reynolds number. The resultant velocity components together with the corresponding isotropic fluctuating velocity components, thus obtained, are summarized in Table 3.6 and Table3.7 as a function of four different locations and three different grid systems (for the two vessels condition). These also include the values of nominal Reynolds number, $Re_{loc,r}$ $\left(\frac{d\rho\sqrt{u^2+v^2}}{\mu}\right)$ and turbulent Reynolds number, Re_t $\left(\frac{d\rho\bar{u}}{\mu}\right)$ for all configurations for three different grid systems. The numerical values of thermophysical properties employed to calculate above dimensionless numbers are presented in Table 3.5.

Table 3.6: Predicted distribution of velocity fields and dimensionless numbers for axisymmetric gas-stirred vessel (L=0.42,R= 0.238 and d=10mm)

grid size	loca tion	z m	r m	$\sqrt{u^2+v^2}$	$\bar{u}$	Re loc	Re_t	Sh exp	Sh pred
	1	0.228	0.104	0.0273	0.0198	273	198	112.7	127.6
24 × 20	2	0.06	0.046	0.0189	0.029	189	290	131.65	131.5
	3	0.383	0.047	0.1147	0.1261	1147	1261	283.9	330.4
	4	0.357	0.106	0.0466	0.0672	466	672	140.0	215.6
	1	0.228	0.104	0.032	0.0533	320	533	112.7	182.3
20 × 16	2	0.06	0.046	0.0243	0.033	243	330	131.65	145.9
	3	0.383	0.047	0.1145	0.1634	1145	1634	283.9	358.8
	4	0.357	0.106	0.0517	0.0972	517	972	140.0	249.0
	1	0.228	0.104	0.0313	0.1065	313	1065	112.7	226.5
15 × 10	2	0.06	0.046	0.0424	0.0875	424	875	131.65	229.2
	3	0.383	0.047	0.065	0.1897	650	1897	283.9	326.7
	4	0.357	0.106	0.034	0.1361	340	1361	140.0	249.8

3.5.1 Estimation of grid size independent solutions

Theoretically predicted flow variables and turbulence parameters in gas stirred vessel are expected to be sensitive to the grid size distribution. It is important to assess the influence of grid size on predicted results. Sherwood numbers have been calculated by using the correlation of Mazumdar et. al. [18] ($Sh = 5.78 Re_{loc,r}^{0.25} Re_t^{0.32}$) for all the conditions and

Table 3.7: Predicted distribution of velocity fields and dimensionless numbers for axisymmetric gas stirred vessel (L=0.21 and R= 0.15)

grid size	location	z m	r m	$\sqrt{u^2+v^2}$	$\bar{u}$	Re loc	Re_t	Sh exp	Sh pred
10×8	1	0.07	0.095	0.00884	0.0361	150	612.69	145	157.7
	2	0.125	0.055	0.029	0.0742	458.37	1173.43	143	256.7
	3	0.04	0.035	0.017	0.0445	273.76	717.27	133	192.8
	4	0.14	0.045	0.0285	0.08	424.36	1191.2	130	253.0
15×10	1	0.07	0.095	0.0108	0.029	183.3	492.18	145	154.6
	2	0.125	0.055	0.0250	0.058	395.15	916.75	143	228.6
	3	0.04	0.035	0.0217	0.0373	349.5	600.68	133	193.6
	4	0.14	0.045	0.036	0.0672	536.04	1000.6	130	253.7
20×16	1	0.07	0.095	0.0078	0.0087	132.38	147.65	145	96.95
	2	0.125	0.055	0.0174	0.0155	275.0	245.0	143	136.86
	3	0.04	0.035	0.0115	0.0059	185.2	95.0	133	91.56
	4	0.14	0.045	0.0297	0.0253	442.2	376.7	130	176.86

compared with corresponding experimental values of Sherwood number. Tables 3.6 and 3.7 provide values of experimental and predicted Sherwood number. It is seen that for the finest grid system only the experimental and predicted values are comparable. Hence, the results deduced via the finest grid systems (20×16 for first vessel (L=0.21,R=0.15) and 24×20 for second vessel (L=0.42,R=0.238)) have been considered for further analysis.

3.5.2 Comparison of numerical prediction with GAs-based correlation

Table 3.8 represents the numerically predicted dimensionless numbers viz., Sh, $Re_{loc,r}$, and Re_t for the optimal grid systems which are essentially reproduced from the previous tables. To assess the adequacy of Eq. (3.6) (mass transfer correlations developed by GAs using experimental data) with reference to the set of numerically predicted results , a log-log plot between the quantities $Sh/Re_{loc,r}^{0.23}$ and $Re_t^{0.35}$ is been shown in Fig. (3.2). The straight line corresponding to the GAs correlation (Eq. (3.6)) is shown together with the numerically predicted results. It is clear that GAs based correlation ($Sh = 6.264 Re_{loc,r}^{0.23} Re_t^{0.35}$) agrees well with the numerically predicted points. Finally,

Table 3.8: Values of dimensionless groups obtained via numerical solution of turbulent Navier-Stokes equation for an optimal grid configuration

Sl. No.	$Re_{Loc,r}$	Re_t	Sh	$\frac{Sh}{Re_{Loc}^{0.22}}$	$\frac{Sh}{Re_{Loc}^{0.23}}$
1	273	198	112.7	32.8	31.0
2	189	290	131.65	41.55	39.43
3	1147	1261	283.9	60.265	56.165
4	466	672	140.0	36.23	34.07
5	132.38	147.65	145.0	49.5	47.13
6	275	245	143.0	41.56	39.3
7	185	95	133.0	42.17	40.02
8	442.2	376.7	130.0	34.03	32.02
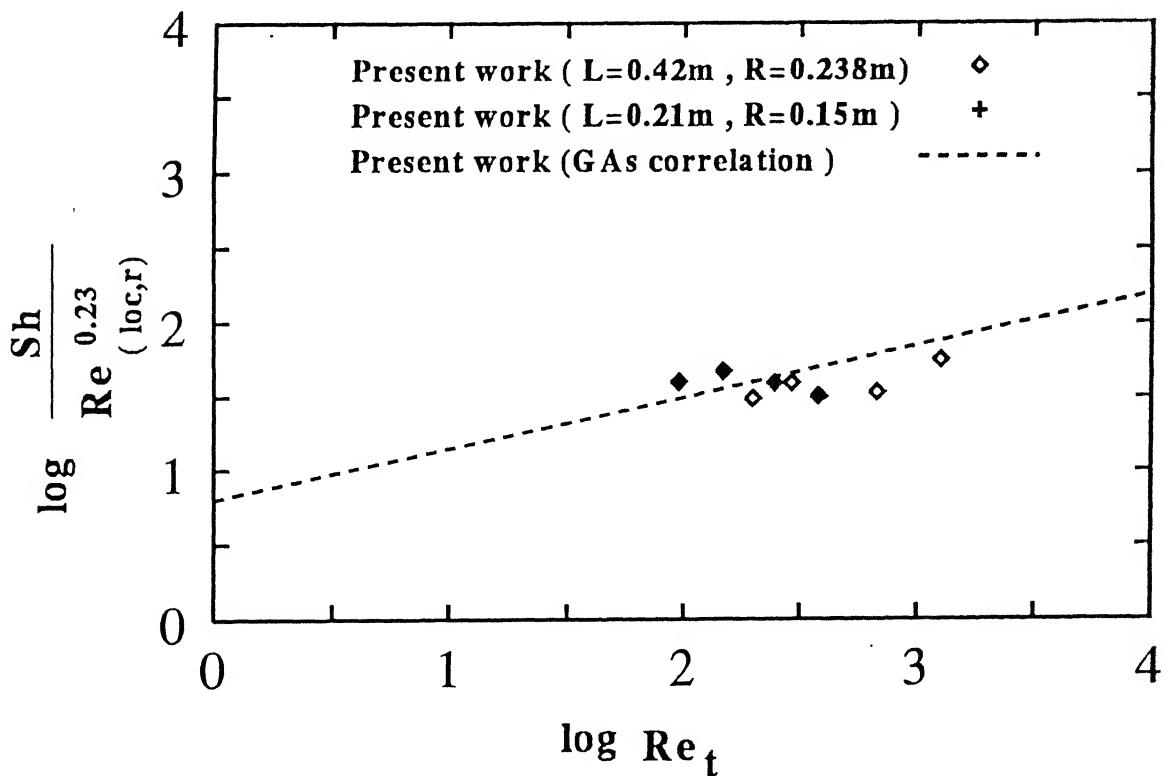
Figure 3.2: Logarithmic variation of $\frac{Sh}{Re_{Loc}^{0.23}}$ and Re_t illustrating the adequacy of GAs mass transfer correlation with reference to the numerically predicted mass transfer rates.

the adequacy of Eq. (3.8) (mass transfer correlation developed by GAs using both experimental and theoretical data Table 3.3) has been assessed in a similar way to that mentioned above. A log-log plot between the quantities $Sh/Re_{loc,r}^{0.22}$ and Re_t has been

shown in Fig. (3.3). This also indicates close agreement between GAs based correlation
and numerically predicted results.
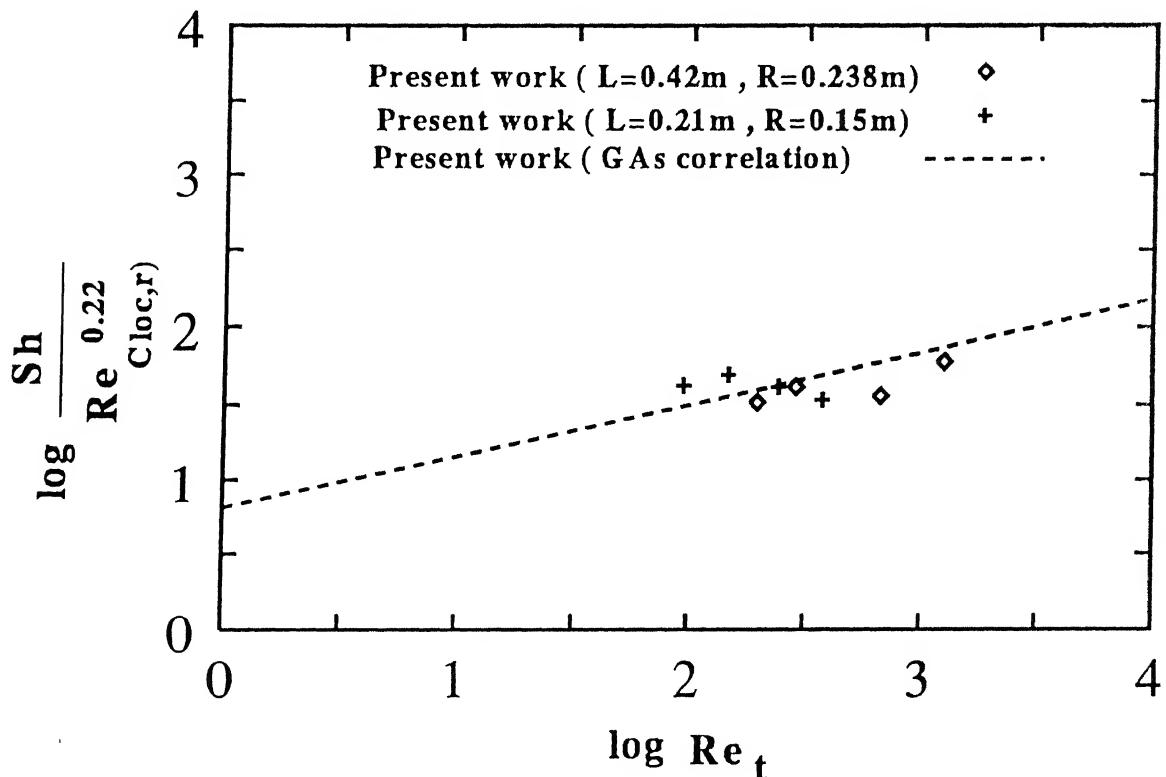
Figure 3.3: Logarithmic variation of $\frac{Sh}{Re_{Loc}^{0.22}}$ and Re_t illustrating the compatibility of GAs mass transfer correlation with reference to the numerically predicted mass transfer rates.

Chapter 4

CONCLUSIONS

The following major conclusions can be drawn from the present investigation regarding mixing time prediction and mass transfer correlation.

4.1 Mixing time prediction

- Mixing rates in gas stirred melts have been theoretically predicted and compared with available experimental results. It is observed that mixing phenomena in such systems can be predicted from the first principles with reasonable accuracy.

- The region close to the bottom of ladle, where flow is relatively weak, exhibited the slowest rate of mixing in the system. This agrees with earlier work [5].

- Numerical results shows that as the liquid depth in the vessel increases the mixing time decreases. The same phenomena is observed in experiments.

- Mixing time depends on the value of empirical constants (d_b, C_b etc.) applied. Hence, for realistic prediction sufficiently accurate information on these are required.

- The spatial variation of mixing is a function of the scale of the vessel and the mixing criteria adopted.

4.2   Mass transfer correlation

- The adequacy of a previously reported mass transfer correlation has been re-examined by the application of Genetic Algorithms. A large number of data reported in the literature on dissolution of vertically submerged solids has been analysed, and an optimal set of values for the pre-exponent and exponent terms derived via GA. The resultant correlation is practically identical to the one determined earlier by Mazumdar et al. by using linear regression.

- Predicted mass transfer rates via the GA based correlation was found to agree well with numerical solution of turbulent Navier-Stokes equation.

Chapter 5

RECOMMENDATIONS FOR FUTURE WORK

The scope of the present work can be further expanded by including the following:

- Mixing time model developed in the present work may be applied to investigate mixing in other configurations of gas stirred bath viz., CAS etc.

- Mass transfer correlation may be assessed against industrial data on dissolution of ferro-alloys etc.

- Application of combined GAs-ANN method remains to be explored to simulate mass transfer from theoretical and industrial data.

Bibliography

[1] Jurgen Mietz and Franz Oeters: *Steel Search*, Vol. 58, No. 10, 1987, p 446.

[2] J. Szekely, T. Lehner and C. W. Chang: *Ironmaking Steelmaking*, Vol. 6, 1979, p 285.

[3] Q. U. Ying, Liang Yun and Liu-Liu: *Proc., Scaninject III*, 1983, 21.1.

[4] M. Salcudean, K. Y. M. Lai and R. I. L. Guthrie: *Can. J. Chem. Eng.*, Vol. 63, 1985, p 51.

[5] D. Mazumdar and Roderick I. L. Guthrie: *Metallurgical Transactions B*, Vol. 17 B, 1986, p 725.

[6] S. Joo and Roderick I. L. Guthrie : *Metallurgical Transactions*, Vol. 23 B, 1992, p 765.

[7] N. El-Kaddah and J. Szekely: *Metallurgical Transactions*, Vol. 6 B, 1981, p 269.

[8] M. Sano and K. Mori: *Trans. Iron Steel Inst. Jpn.*, Vol. 23, 1983, p 10.

[9] T. Stapurewicz and Nicolas J. Themelis : *Canadian Metallurgical Quarterly*, Vol. 26, No. 2, 1987, p 123.

[10] G. G. Krishnamurthy, S. P. Mehrotra and A. Ghosh: *Metallurgical Transactions*, Vol. 20 B, 1989, p 53.

[11] G. G. Krishnamurthy: *ISIJ International*, Vol. 29, 1989, p 49.

[12] W. J. Lavender and D-C. T. Pei: *Int. J. of Heat and Mass Transfer*, Vol. 10, 1967, p 529.

[13] S. Taniguchi, M. Ohmi, S. Ishiura and S. Yamauchi: *Transactions ISIJ*, Vol. 23, 1983, p 565.

[14] S. Taniguchi, M. Ohmi and S. Ishiura: *Transactions ISIJ*, Vol. 23, 1983, p 571.

[15] S. Whitaker: *Journal of A. I. Ch. E.*, Vol. 18, 1972, p 361.

[16] J. Szekely, J.H. Grevet and N. El-Kaddah: *Int. J. Heat Mass Transfer*, Vol. 27, No. 7, 1984 , p 1116.

[17] D. Mazumdar, S. K. Kajani and A. Ghosh : *Steel Search* , Vol. 61, 1990, p 339.

[18] D. Mazumdar, N. Kumar and V. Verma: *Ironmaking and Steelmaking*, Vol. 19, No. 2, 1992, p 152.

[19] D. Mazumdar, Tanuj Narayan, and Paramjit Bansal: *Appl. Math Modelling*, Vol. 16, 1992 (May), p 255.

[20] J. K. Wright: *Metallurgical Transactions*, Vol. 21B, 1990.

[21] J. K. Wright and I. F. Taylor: *ISIJ International*, Vol. 33, 1993, p 529.

[22] S. Asai, M. Kawachi and I. Muchi: *Scaninject III*, 1983, 12.1.

[23] S.C. Koria : *Steel Research*, Vol. 59, 1988, p 489.

[24] D. Mazumdar and R. I. L. Guthrie: *Metallurgical Transactions*, Vol. 24B, 1993, p 649.

[25] G. II. Geigor and D. R. Poirier: *Transport Phenomena in Metallurgy*, Massachusetts, Addison Wesley Publishing Co. (1973).

[26] D. Mazumdar and Roderick I. L. Guthrie: *ISIJ International*, Vol. 34, No. 5, 1994, p 384.

[27] B. E. Launder and D. B. Spalding: *Computer Methods in Applied Mechanics an* *Engg.*, Vol. 3, 1974, p 269.

[28] S. V. Patankar: *Numerical Heat Transfer and Fluid Flow*, Hemisphere Pub. Inc New York (1900).

[29] S. T. Johansen and F. Boysan : *Metall. Transactions*, Vol. 19 B, 1988, p 755.

[30] K. Deb: *Optimization For Engineering Design* , Prentice-Hall of India, New Delhi (1995).

[31] D. E. Goldberg: *Genetic Algorithms in search, optimization and machine learning,* Reading, MA, Addison-Wesley, (1989).

[32] D.E. Goldberg and K. Deb: *A comparative analysis of selection schemes used in genetic algorithms* , Foundations of Genetic Algorithms, San Matco CA, Morgan Kaufman, 1991, p 69.

[33] A. K. Singh and D. Mazumdar: *Metallurgical and Materials Transaction B*, Vol. 28B, 1997 , p 95.

[34] R. B. Bird, W. E. Stewart, and E.N. Lightfoot: *Transport Phenomena*, John Wiley and Sons Inc. New York (1960).

[35] D. Mazumdar and Roderick I. L. Guthrie: *ISIJ International*, Vol. 35 (1995), No. 1, p 1.

123733

Date Slip

This book is to be returned on the
date last stamped.

123733

· ·

· ·

· ·

· ·

· ·

· ·

· ·

· ·

· ·

· ·

· ·

· ·

MME - 1997 - M - KUM - MOD